The nuclear GAPDH-HMGB cascade in cortical microglia regulates cognitive flexibility

Adriana Ramos[1#], Koko Ishizuka[2#], Ho Namkung[1,3], Lindsay N. Hayes[1], Atsushi Saito[2], Ayesha Sengupta[9], Rupali Srivastava[2], Coleman Calva[10], Arisa Hayashida[2], Noah Elkins[2], Trexy Palen[2], Elisa Carloni[2], Tsuyoshi Tsujimura[2], Juan A. Gallego[11], Delbert G. Robinson[11], Anil K. Malhotra[11], Satoshi Ikemoto[10], Rana Rais[5,6], Barbara S. Slusher[1,2,5,6,7], Minae Niwa[2], Toshiaki Saitoh[12], Eiki Takimoto[7],and Akira Sawa[1,2,3,4,5,8*]

Departments of [1]Neuroscience, [2]Psychiatry, [3]Biomedical Engineering, [4]Genetic Medicine, [5]Pharmacology, [6]Neurology, [7]Medicine, Johns Hopkins University School of Medicine, Baltimore, MD 21287, USA

[8]Department of Mental Health, Johns Hopkins University Bloomberg School of Public Health, Baltimore, MD 21287, USA

[9]Behavioral Neurophysiology Neuroscience Section, [10]Neurocircuitry of Motivation Section, National Institute on Drug Abuse, Baltimore, MD 21224, USA

[11]Zucker School of Medicine at Hofstra/Northwell, Hempstead, NY 11549, USA

[12]Nihon Pharmaceutical University, Saitama, 362-0806, Japan

[#]Equal contribution

*Correspondence: asawa1@jhmi.edu

SUMMARY

We report a molecular mechanism that controls brain response to stress and regulates adaptive behavior. In a mouse model under subacute stress, activation of the nuclear glyceraldehyde dehydrogenase (N-GAPDH) cascade occurs selectively in cortical microglia. This stress response causally underlies cognitive inflexibility in mouse behaviors, which is proven by pharmacological intervention or microglia-specific genetic intervention targeting the initial steps of the N-GAPDH cascade. We performed ChIP-Seq against N-GAPDH and for the first time demonstrate how N-GAPDH influences the genome-wide transcriptional landscape under stress. Through this analysis, we obtained evidence that High-Mobility Group Box (HMGB) downstream of the N-GAPDH cascade, connected with the NMDA receptor, is responsible for the regulation of the adaptive behavior. Furthermore, the activation of this N-GAPDH-HMGB cascade is reflected by augmented autofluorescence in peripheral blood cells. Consistent with these observations, we clinically demonstrated an association between augmented lymphoblast autofluorescence and impaired cognitive flexibility in patients with schizophrenia.

Keywords

GAPDH, transcriptional regulation, ChIP-seq, cognitive flexibility, microglia, HMGB, NMDA receptors, autofluorescence, schizophrenia

INTRODUCTION

How an organism responds to stress is a central question in biology. The brain is an organ that senses and copes with stress, which is reflected in behavioral changes of the organism. The brain includes many cell types, and a key question is which molecular cascade(s) in which specific cells sense stress and mediate the stress response. Among representative stress-triggered intracellular signaling, we have studied a cascade in which glyceraldehyde-3-phosphate dehydrogenase (GAPDH) acts as a sensor of cellular stress (Shahani and Sawa, 2011; Tristan et al., 2011). The present study reports a novel molecular landscape involving GAPDH at the whole genome level and shows the causal involvement of GAPDH in the brain response to stress.

GAPDH was simply recognized as a house keeping molecule as a glycolytic enzyme. However, recent studies have demonstrated that GAPDH is a multi-functional protein (Chang et al., 2013; Tristan et al., 2011). Beyond its classic role in glycolysis, during stress, GAPDH is post-translationally modified at specific residues, such as cysteine 150 (Cys-150) and lysine 160 (Lys-160), which converts this glycolytic enzyme into a signaling molecule (Hara et al., 2005). S-nitrosylation (or possibly oxidation) at Cys-150 allows post-translationally modified GAPDH to interact with a chaperon protein Siah1 creating a protein complex of GAPDH-Siah1. Through this process, GAPDH loses its glycolytic activity and is translocated to the nucleus as a GAPDH-Siah1 complex (Hara et al., 2005). The nuclear translocation of a pool of GAPDH implies a gain-of function that has a significant impact on cellular signaling, whereas a loss-of-function of 1-2% of the total glycolytic activity due to this conversion is negligible on overall cell metabolism (Hara et al., 2005).

Accordingly, GAPDH-Siah1 protein binding is a key regulatory process that initiates the nuclear-GAPDH (N-GAPDH) cascade, which can be selectively blocked by several compounds without affecting the glycolytic activity of GAPDH. These selective blockers include structural analogues of deprenyl (e.g., CGP 3466B) (Hara et al., 2006). We have recently reported that (1R, 3R)-1, 3-dimethyl-2-propargyl-1, 2, 3, 4-tetrahydroisoquinoline (designated as RR in this study) is a deprenyl structural analogue with the highest potency among the analogues, as far as we are aware, for blocking the GAPDH-Siah1 protein interaction (Zhang et al., 2022). Our group also reported that the replacement of lysine 225 for alanine (K225A) on GAPDH abolished GAPDH-Siah1 binding (Hara et al., 2005). Although this cascade has been mainly studied in the context of cell death (Guha et al., 2016), activation of the N-GAPDH cascade was also reported in animal models that do not accompany cell death (Johnson et al., 2013). Two major knowledge gaps exist in the current understanding of the N-GAPDH cascade. First, the precise mechanism of N-GAPDH in the nucleus remains to be elucidated, although N-GAPDH has been suggestively involved in the regulation of gene transcription (Tristan et al., 2011). An unbiased, genome-wide approach is warranted to account for a wider implication of the N-GAPDH cascade beyond cell death. Second, although the N-GAPDH cascade may mediate the stress response, the causal link from the molecule to behavior has not been fully achieved yet.

In order to respond to stress properly, cognitive flexibility is required for the organism. Cognitive flexibility is a construct of executive function that adapts our decision-making to new experiences (Ionescu, 2012). This behavioral construct is closely related to creativity and empathy, enabling us to not only adapt, but also to think outside of the box, taking other perspectives into consideration (Ionescu, 2012). Cognitive flexibility is predominantly regulated

by the prefrontal cortex (Cho et al., 2015; Stokes et al., 2017). This function is sensitive to, and negatively affected by, conditions of stress (Arnsten, 2009; Diamond, 2013; Plessow et al., 2011). Accordingly, cognitive inflexibility is frequently observed in an array of brain disorders, including schizophrenia (SZ) and Alzheimer's disease (AD) (Baudic et al., 2006; Floresco et al., 2009; Gruber et al., 2010). In these conditions, impairment of cognitive flexibility directly leads to functional deficits and worsens clinical outcomes for patients (Malloy and McLaughlin, 2010; Marshall et al., 2011). Nevertheless, pathophysiological mechanisms for this impairment at the molecular and cellular levels remain to be elucidated. Cognitive flexibility is assessed with the Wisconsin Card Sorting Test (WCST) in clinical settings, and deficits in the WCST are well established in patients with SZ and in a portion of patients with AD (Berman et al., 1985; Callicott, 2000; Nagahama et al., 2003). Similarly, the attentional set-shifting task has been used to test this behavioral construct in rodent models (Bissonette et al., 2008; Cho et al., 2015; Scheggia et al., 2014). This task consists of an initial association followed by rule shifting, the latter of which is used to evaluate cognitive flexibility (Cho et al., 2015; Scheggia et al., 2014). An NIH-supported consortium that assessed comparative construct validity and test batteries translatable between rodents and humans has reported the WCST and rule-shifting as analogous tasks to study cognitive inflexibility (Moore et al., 2013).

In the present study, we aimed to address the aforementioned two knowledge gaps. To address these questions, we used a mouse model with cognitive inflexibility in which we observed the N-GAPDH cascade selectively activated in cortical microglia. The cognitive deficits were reverted with pharmacological intervention or microglia-specific genetic intervention targeting the initial steps of the N-GAPDH cascade. Through whole genome chromatin immunoprecipitation

sequencing (ChIP-Seq), we provided the transcriptional landscape that was regulated by N-GAPDH in stressed microglia. Through this analysis, we obtained evidence that High-Mobility Group Box (HMGB) downstream of the N-GAPDH cascade, in conjunction with its activation of the NMDA receptor, is responsible for the regulation of adaptive behaviors. Finally, we found this mouse model also displayed activation of the N-GAPDH cascade in peripheral blood mononuclear cells (PBMCs), which was correlated with an increase in cellular autofluorescence (AF). Consistent with these observations, we clinically demonstrated that an augmented AF in lymphoblasts from humans was correlated with impaired cognitive flexibility, with evidence that the altered AF was also associated with the N-GAPDH-HMGB cascade.

RESULTS

The N-GAPDH cascade underlies cognitive inflexibility in a stress-induced mouse model

To demonstrate that the N-GAPDH cascade can play a mechanistic role linking stress and behavior at the molecular level, we used a mouse model repeatedly treated with a low dose of LPS [low-dose stressors (LPS) at multiple times: LSM model] (**Figure 1A**). We observed an excess of oxidative stress and activation of the N-GAPDH cascade in the brains of LSM mice (**Figures S1A and S1B**). In contrast, we did not observe any sign of blood brain barrier damage, nor cell death in the brain (**Figures S1C-S1F**). Signs of sickness behavior were not present 24 h after treatment (Dantzer et al., 2008), when all biochemical or behavioral outcomes were recorded. No changes in locomotor and swimming activity were observed in LSM mice compared to control mice (**Figures S1G and S1H).** However, LSM mice presented significant deficits in cognitive flexibility as measured by the attentional set-shifting task, but showed no impairment in learning the initial association portion of the task (**Figures 1A-1C, and S1I**).

Moreover, we observed that LSM mice performed more perseverant errors than control mice (**Figure 1D**). These results allowed us to conclude that LSM mice were less flexible, requiring more attempts in order to disengage from the paradigm that they learned during the initial association.

To test whether the N-GAPDH cascade is involved in the regulation of this cognitive construct, we used the RR pharmacological compound to specifically block activation of the N-GAPDH cascade by interfering with the binding of GAPDH and Siah1, without affecting the glycolytic activity of GAPDH and monoamine oxidase. We confirmed *in vitro* that this compound blocked the GAPDH-Siah1 protein interaction more potently than other drug analogs (**Figure S2A**). In addition, we demonstrated that RR reached the brain when it was systemically injected, and even displayed a unique enrichment in the brain (**Figure S2B**). Therefore, we systemically administered the RR compound in LSM mice to evaluate its impact on behavioral flexibility. We confirmed at the tissue level that initiation of the N-GAPDH cascade was blocked by the systemic injection of RR, as shown by the absence of nuclear translocation of GAPDH in the brain of LSM mice treated with RR (RR LSM mice) (**Figure S1B**). Interestingly, the RR injection also successfully blocked the behavioral deficits seen in the rule-shifting paradigm. In particular, RR significantly reduced the number of perseverant errors (**Figures 1C and 1D**). These results indicate that the N-GAPDH cascade is activated in response to LSM treatment and underlies cognitive inflexibility.

Stress-induced upregulation of the N-GAPDH cascade occurs selectively in microglia

Since activation of the N-GAPDH cascade was responsible for the behavioral inflexibility deficits observed in LSM mice, we decided to determine the cellular specificity of the N-GAPDH activation. We focused on microglia and astrocytes because they are the main cell types involved in the provocation and resolution of inflammatory and oxidative stress related processes in the brain (Colombo and Farina, 2016; Colonna and Butovsky, 2017; Sochocka et al., 2017). Interestingly, we observed a significant upregulation of N-GAPDH only in microglia cells, as reflected by an increased binding of GAPDH and Siah1 in microglia (**Figures 2A and 2B**). A specific antibody against sulfonation of GAPDH at cysteine-150 (SulfoGAPDH Ab) (Hara et al., 2005; Sen et al., 2008) also confirmed activation of this cascade in microglia in the medial prefrontal cortex (**Figures 2C and S3A**), but not in astrocytes or neurons. Nuclear fractionations proved the presence of GAPDH in the nuclei of microglia cells (**Figure S3B**). Furthermore, we observed activation of this cascade in cortical but not striatal microglia (**Figure 2D**). As expected, systemic administration of the RR compound blocked activation of the N-GAPDH cascade in microglia (**Figure 2E**).

In addition to the pharmacological intervention by RR, we generated a conditional mouse model designed to disrupt GAPDH-Siah1 binding and thus prevent activation of the N-GAPDH cascade under stressors (Zhang et al., 2022). We previously published that a point mutation that replaces lysine 225 of GAPDH with alanine (K225A) can abolish the GAPDH-Siah1 binding without affecting other key features of GAPDH, including its glycolytic activity (Hara et al., 2005; Zhang et al., 2022). To specifically block the N-GAPDH cascade in microglia in the central nervous system, we generated GAPDH-K225A$^{\text{Cx3cr1-CreER}}$ knockin mice (K225A-MG mice). As expected, we did not observe an upregulation of the N-GAPDH cascade in these knockin mice

even when these mice were repeatedly treated with LPS (K225A-MG LSM) (**Figure S3C**). Further, this microglia-specific genetic manipulation to block the N-GAPDH cascade successfully prevented the behavioral deficits in the rule-shifting paradigm including a reduced number of perseverant errors in K225A-MG LSM mice (**Figure 2F and 2G**).

Whole-genome landscape of transcriptional regulation by the N-GAPDH cascade

The above results in LSM mice show that activation of the N-GAPDH cascade specifically in microglia of the medial prefrontal cortex causally underlies the stress-elicited cognitive deficits. We hypothesized that N-GAPDH would regulate gene transcription, which in turn results in crucial stress responses. To address this question, we performed ChIP-Seq against N-GAPDH in cortical microglia from LSM mice by using a specific antibody against acetylated GAPDH at Lys-160 (**Figure 3A**). This approach allowed us to specifically target a sub-pool of GAPDH that is actively translocated to nuclei, reflecting activation of the N-GAPDH cascade (Colell et al., 2009; Tristan et al., 2011). We hypothesized that N-GAPDH might interact with the transcriptional machinery, regardless of whether the protein directly interacts with chromatin, and then regulate gene transcription. In order to efficiently achieve immunoprecipitation of the chromatin-protein complex, we treated *ex vivo* microglia cells with 2 mM disuccinimidyl glutarate to initially crosslink protein complexes, followed by formaldehyde treatment to covalently link protein complexes to DNA for the ChIP (Lee et al., 2006; Nowak et al., 2005). Using this approach, we found 721 peaks of N-GAPDH occupancy distributed throughout the genome (**Figure 3B**).

In order to address the nucleotide sequences that N-GAPDH has avidity for, we performed motif-enrichment and motif-discovery analyses by using the MEME Suite 5.0.5 pipeline (Ma et al., 2014). The top hits found in these analyses were motifs already described for other transcriptional immune regulators such as signal transducer and activation of transcriptions (STAT) (Ihle, 1996) and interferon regulator factors (IRF) (Tamura et al., 2008) (**Figures 3C and 3D**). Additionally, some of the motifs indicated in the ChIP-seq for N-GAPDH were highly similar to already described motifs for Sall1 **(Figure 3C**), one of the most important transcription factors that defines microglia identity and function (Buttgereit et al., 2016). These results fit with the notion that GAPDH may be exerting its transcriptional function as part of a transcriptional complex.

To further evaluate our data, we used the list of genes from the peaks that relied on non-gene desert areas to perform an ingenuity pathway analysis (IPA). The top 5 canonical pathways obtained in this study are presented in **Figure 3E**. First, we observed that N-GAPDH regulates the stress response of the endoplasmic reticulum (ER) by binding to the promoter regions of genes such as Xbp1, Atf6, and Map3k5. N-GAPDH also regulates its own expression and the expression of other important glycolytic enzymes such as lactate dehydrogenase C. These data indicate that the N-GAPDH cascade may transcriptionally connect the stress and metabolic cascades in a cell autonomous fashion. In addition, we also observed HMGB signaling as one of the top pathways. Some studies have reported that HMGB proteins are actively released from microglia (Lee et al., 2014; Shi et al., 2018), whereas other reports demonstrated that HMGB proteins can regulate NMDA-glutamate receptors (Fu et al., 2017; Nestor et al., 2018; Pedrazzi et al., 2012). Particularly, HMGB1 has been described to directly bind with the GluN1 and GluN2B

subunits of NMDA receptors and act as an agonist (Nestor et al., 2018; Pedrazzi et al., 2012). Considering that deficits in the NMDA receptors are well known to underlie cognitive dysfunction and mental conditions (Carlén et al., 2012; Cissé et al., 2011; Jackson et al., 2004), we decided to further question whether microglial HMGB and neuronal NMDA receptors are functionally associated, as a possible mechanism of microglia-neuronal communication in conjunction with the N-GAPDH cascade in microglia.

N-GAPDH regulation of HMGB signaling in microglia

To address the question of how the N-GAPDH cascade plays a mechanistic role in linking stress to behavior *in vivo*, we hypothesized that HMGB signaling in microglia was a modulator of NMDA receptor-mediated neuronal activity. To address this question, we conducted ChIP-qPCR to confirm that the N-GAPDH protein complex bound to the promoter region of HMGB2 in cortical microglia, and indeed this interaction was confirmed in LSM mice (**Figures 4A and 4B**). Consistent with this data, HMGB2 mRNA was upregulated in LSM mice (**Figure 4C**). These pathological changes were normalized by pharmacological treatment with RR (**Figures 4B and 4C**).

HMGB1 and HMGB2 are highly homologous proteins (Štros, 2010) with the capacity to interact and form a complex (Barreiro-Alonso et al., 2016; Ruepp et al., 2009; Štros, 2010), which we confirmed by our experiments (**Figure S4A**). Furthermore, their expressions are reportedly mutually regulated (Barreiro-Alonso et al., 2019; Ronfani et al., 2001); for example, the specific knockdown of HMGB2 reduced the expression of HMGB1. Considering this regulatory mechanism, we decided to test the expression of HMGB1 protein in our model. Consistent with

the theory built by published reports (Barreiro-Alonso et al., 2016, 2019; Ronfani et al., 2001; Ruepp et al., 2009; Štros, 2010), in LSM mice in which HMGB2 is upregulated, both HMGB1 and HMBG2 were augmented at the protein level (**Figure 4D**). Importantly, pharmacological treatment with RR significantly blocked the upregulation of both proteins (**Figure 4D**), whereas treatment with RR in control mice (without LPS) did not affect the level of these proteins (**Figure S4B**). In K225A-MG LSM mice, there was no upregulation of HMGB2 mRNA (**Figure 4C**) and HMGB1/2 proteins (**Figure 4D**), which are consistent with results from RR treated LSM mice. Note that K225A-MG mice themselves did not show a difference in the level of HMGB1/2 proteins compared with control [Cx3cr1-CreER; WT-GAPDH] mice (**Figure S5**).

HMGB proteins are known to be released into the extracellular space in a passive or active manner (He et al., 2017). Passive release involves processes of regulated cell death (He et al., 2017), while active release is mediated through secretory lysosomes (Gardella et al., 2002; He et al., 2017). Since we did not observe programmed cell death in microglia from LSM mice (**Figure S1F**), we hypothesized that HMGB proteins were actively secreted from microglia into the extracellular space in LSM mice. To test this hypothesis, we quantified the percentage of HMGB protein inside the lysosomes of microglia using 3D reconstruction from confocal images. This analysis revealed an increase in HMGB proteins inside microglial lysosomes of LSM mice, which was reversed with RR pharmacological treatment and genetic intervention (**Figures 4E and S6)**.

HMGB secreted from microglia modulates neural activity without causing excitotoxicity

Next, we questioned how the change in expression of HMGB proteins mediated by N-GAPDH in microglia might affect neural function. HMGB1 has been reported to bind and modulate the GluN1/GluN2B subunits of the NMDA receptors (Fu et al., 2017; Pedrazzi et al., 2012). Thus, we decided to monitor the possible impact of HMGB1 on the NMDA receptors of pyramidal neurons, in which GluN2B is preferentially expressed (Bygrave et al., 2019; Paoletti et al., 2013), by measuring neuronal activity through calcium imaging. Given that disinhibition of glutamatergic pyramidal neurons and a subsequent increase in glutamate synaptic activity has causally underlaid cognitive flexibility deficits in past reports (Jackson et al., 2004; Mohn et al., 1999), we hypothesized that HMGB1 triggered by the microglial N-GAPDH cascade hyperactivates the pyramidal neurons in LSM mice with behavioral deficits.

To address this question, we used mice that selectively expressed GCaMP6s in VGlut1-positive excitatory neurons and specifically focused on layer 5 (L5) in the medial prefrontal cortex (the prelimbic area), a region known to be involved in cognitive flexibility in mice (Cho et al., 2015). To assess the spontaneous activity of individual excitatory neurons, we used a constrained non-negative matrix factorization algorithm optimized for slice imaging that allowed us to determine the frequency and amplitude of calcium events (**Figure 5A; Video S1**). Calcium transients in the prelimbic L5 excitatory neurons were more frequent in LSM compared with control mice, whereas amplitude levels were similar (**Figure 5B**). These data indicate a plausible increase in neuronal activity and an overall cytosolic calcium overload in LSM excitatory neurons. As shown before, no neuronal cell death was observed in LSM mice (**Figure S1F**). Treatment of LSM mice with RR ameliorated the increased frequency of calcium transients, suggesting a causal involvement of microglial activation of the N-GAPDH cascade (**Figure 5B**).

Additionally, application of an antibody against HMGB1 resulted in a neutralizing effect on neuronal firing rates and normalization in the frequency of calcium transients (**Figure 5B**). Furthermore, the use of K225A-MG LSM mice that selectively expressed GCaMP6s in Thy1-positive excitatory neurons proved the causal effect of the microglial N-GAPDH cascade in the increased frequency of calcium transients (**Figure 5C**). In contrast, the frequency of calcium transients and amplitude levels were not different in the prelimbic L5 VGAT-positive inhibitory neurons between control and LSM mice expressing GCaMP6s in VGAT-positive inhibitory neurons (**Figure 5D**). We also approached this question by whole-cell patch clamp recordings and observed that prelimbic L5 excitatory neurons in LSM mice showed significantly higher peak inward NMDA receptor-mediated current than control mice or K225A-MG LSM mice (**Figure 5E**). These data also indicate an increase in NMDA receptor-mediated excitation in the prelimbic L5 excitatory neurons of LSM mice, which is normalized by genetic intervention with the N-GAPDH cascade in microglia.

Peripheral blood cell autofluorescence in association with the N-GAPDH cascade: its correlation with cognitive flexibility in mice and humans

The involvement of stress-associated cascades in cognitive deficits has been clinically suggested through many descriptive studies that correlate the cognitive deficits to stress-associated molecules, such as reactive oxygen species, glutathione, cytokines, and complement, in patient biofluids and blood cells (Coughlin et al., 2013, 2017; Hampel et al., 2018; Hayes et al., 2014; Krance et al., 2019; Landek-Salgado et al., 2016; Newton et al., 2017; Orlovska-Waast et al., 2019; Tanaka et al., 2017; Upthegrove and Khandaker, 2020). However, it remains elusive how such molecular changes can underlie cellular pathology, circuitry changes, and cognitive deficits.

The combination of clinical observations and preclinical studies in animal models connecting peripheral and brain changes at the mechanistic level may be key to address this question.

Accordingly, we questioned whether the N-GAPDH cascade was activated not only in microglia but also in peripheral blood mononuclear cells (PBMCs) in LSM mice that show cognitive inflexibility. We observed that the N-GAPDH cascade was also activated in PBMCs from LSM mice (**Figure S7A**). Activation of N-GAPDH was further validated by assessing HMGB1 and HMGB2 protein expression, which was also augmented in LSM mice (**Figure 6A**). To our surprise, activation of the N-GAPDH cascade in PBMCs was accompanied by an increase in the level of autofluorescence (AF) emitted by these cells (**Figures 6B and S7B**). Note that propidium iodide-positive dead cells were removed from all the analyses (**Figure S7B**).

As described above, the genetic abolishment of GAPDH-Siah1 protein binding (K225A-MG) blocked activation of the N-GAPDH cascade. To address whether activation of the N-GAPDH cascade and subsequent upregulation of HMGB proteins underlie the increased AF in PBMCs, we used this genetic intervention in blood cells by generating GAPDH-K225A$^{CMV\text{-}Cre}$ knockin mice (K225A-Pan mice). We confirmed that the genetic intervention in K225A-Pan LSM mice abolished the upregulation of the N-GAPDH cascade and HMGB1/2 proteins in PBMCs (**Figures 6A and 6C**). Importantly, the aberrant increase in the level of AF in PBMCs was also ameliorated in K225A-Pan LSM mice (**Figure 6B**), suggesting that a significant portion of AF from LSM PBMCs is N-GAPDH-derived.

Next, we hypothesized that the augmented AF in peripheral blood cells might be associated with cognitive inflexibility in humans. To test this notion, we examined the level of AF in lymphoblasts from healthy controls and patients with SZ, a typical condition that displays cognitive inflexibility, and correlated these findings with a set of neurocognitive functions (**Figure 7A**). We observed a specific association between the level of AF and executive function, a neurocognitive dimension determined by the WCST, after adjusting for multiple comparisons and potential confounding factors (**Figures 7B, 7C, and S7C**). To address confounding effects of antipsychotic medication, we examined the level of AF in an independent, longitudinal cohort of first episode SZ patients. In this cohort, all patients had at most only a two-week lifetime exposure to antipsychotics at the time of the first sample collection, followed by another sample collection after 52 weeks of treatment with an antipsychotic medication . When we compared AF in lymphoblasts from this cohort, we did not observe any significant differences in AF between pre- and post-treatment sample collections (**Figure 7D**), indicating that the effect of antipsychotic medications is negligible. To obtain evidence that this stress cascade indeed underlies the increased AF in human lymphoblasts, we examined the levels of HMGB proteins and AF in parallel, and observed that AF was significantly correlated with HMGB1 (**Figures 7E and S7D**). Together, activation of the N-GAPDH cascade followed by the GAPDH-HMGB signaling cascade is likely to underlie AF and cognitive flexibility not only in mouse models but also in humans.

DISCUSSION

We report a novel mechanism for the transcriptional response to stressors mediated by N-GAPDH. In the medial prefrontal cortex this stress response occurs selectively in microglia.

Upregulated HMGB proteins are released from microglia and influence adjacent neuron activity, which in turn affects cognitive flexibility, a cognitive construct relevant to a wide range of neuropsychiatric disorders. This stress response mediated by N-GAPDH also occurs in PBMCs. AF in blood cells may be a candidate for a high-throughput surrogate marker that mirrors this N-GAPDH stress response associated with cognitive inflexibility in humans.

The ChIP-Seq data presented here provides a general landscape for how N-GAPDH mediates stress-triggered gene transcription at the whole genome level, and further elucidates a specific novel mechanism that underlies cognitive inflexibility in a cell non-autonomous mechanism between microglia and neurons. Subsets of genes governed by N-GAPDH include those that play a central role in cell autonomous homeostatic regulation. For example, N-GAPDH is likely to regulate genes that are known to be involved in the ER stress response. It is interesting to postulate the biological merits in the novel cross-talk among homeostatic signaling pathways: a glycolytic enzyme senses redox imbalance, which converts the enzyme into a signaling molecule that translocates to the nucleus, where it is subsequently involved in the transcriptional regulation of proteostatic balance (Balch et al., 2008).

We also found that N-GAPDH regulated the expression of GAPDH itself in a feedback loop mechanism. Previous studies have described that the HIF-α and mTOR pathways directly regulate transcription of glycolytic enzymes in an array of conditions from hypoxia to immune activation (Cheng et al., 2014; Semenza et al., 1994). Positive feedback mechanisms are in general highly effective for cells to achieve flexible and quick responses, and to maintain homeostasis (Hancock et al., 2017; Jones, 1965). Nuclear localization of many glycolytic

enzymes has been reported mainly in cancer research, but their roles remain elusive. Glycolytic proteins may orchestrate their gene transcription, at least in part, through the N-GAPDH cascade.

In this study, we discovered that N-GAPDH transcriptionally regulates HMGB2, driving the upregulation of HMGB proteins in microglia. Additionally, we provided evidence that these proteins can pathologically regulate neural circuitries without cell death. This contrasts with previous reports on the pathological roles in epilepsy, traumatic brain injury, lupus, ischemic stroke, and sepsis, in which HMGB proteins function as drivers of inflammatory and immune processes in the context of massive cell death (Kim et al., 2018, 2006; Muhammad et al., 2008). Instead, in this study, the agonistic effect of HMGB proteins on the NMDA receptors of pyramidal neurons leads to a direct increase in neuronal excitatory activity. This net increase in excitatory activity would subsequently lead to behavioral inflexibility. This is consistent with past literature that reported inflexible behavior elicited by ketamine or MK-801: these compounds are believed to inhibit NMDA receptors in fast-spiking interneurons, which in turn leads to disinhibition or increased net excitation in the prefrontal cortex (Bygrave et al., 2019; Moghaddam and Javitt, 2012; Moghaddam and Krystal, 2012; Paoletti et al., 2013).

Recent studies in neuropsychiatry have established a concept that neuropsychiatric conditions are systemic (Kirkpatrick et al., 2014; Morris et al., 2014). In the present study, we observed that activation of the N-GAPDH cascade, and downstream targets, occurs in both cortical microglia and PBMCs. It is interesting that peripheral immune cells reflect critical changes happening in cortical microglia (Prinz and Priller, 2014). To develop biomarkers, it is important to consider

whether the brain/peripheral relationship is mere correlation or based on an established mechanism. Our study may provide a prototype to develop similar studies linking brain pathology and peripheral changes. It also contributes to the establishment of high-throughput biomarkers, by correlating levels of AF in peripheral blood cells to specific dimensions of cognitive dysfunction. Evaluating brain dysfunction by quantitative markers such as AF is an important translational aspect to the future of psychiatry. Cellular AF can be utilized in a high throughput manner, as it is measurable by a plate reader or other methods. Ideally, the quantitative nature of AF may detect a very subtle early stage of cognitive decline that may not be noticeable using descriptive neuropsychological testing.

Altogether, we provide a novel conceptual framework that an enzyme, which is traditionally considered for cellular homeostasis through glycolysis, transcriptionally regulates microglial function for adaptive behavior in response to stressors. We speculate that GAPDH is not the only enzyme to have such a unique role. The nuclear localization of other glycolytic enzymes has been historically reported (Boukouris et al., 2016; Yu and Li, 2017), however, their role as transcriptional regulators remains elusive. We believe that the present study represents the tip of the iceberg for a higher level mechanism that involves the transcriptional regulation of homeostasis by bioenergetic enzymes, a mechanism that has probably evolved from cellular to complex systems.

MATERIALS and METHODS

Antibodies and reagents. All reagents were purchased from Sigma Aldrich with the exception of: TUNEL Assay Kit-FITC (Abcam, ab66108), DNA SMARTTM ChIP-Seq Kit (Takara,

634865), Adult Neural Dissociation kit (Miltenyi Biotec, 130-107-67), CD11b MicroBead Kit (Miltenyi Biotec, 130-107-677), Anti-ACSA-2 MicroBead Kit (Miltenyi Biotec, 130-097-679), and ArcturusTM Pico PureTM RNA isolation kit (Thermo Fisher Scientific, KIT0240).The following antibodies were used: anti-sulfonated-GAPDH (Cys152) (Research Genetics), anti-acetyl-GAPDH (Lys160) (Millipore Sigma, 07-2184), Anti-GAPDH (Santa Cruz Biotech, sc-32233), anti-HMGB1 (Abcam, ab18256), anti-HMGB2 (Abcam, ab67282), anti-H3 (Abcam, ab18251), anti-P84 (GeneTex, GTX70220), anti-Siah1 (Santa Cruz Biotech, sc-5506), Anti-NeuN (Millipore Sigma, MAB377), anti-Aldh1l1 (Millipore Sigma, MABN495), anti-Iba1 (Wako, 016-20001), anti-CD68 (AbD Serotec, MCA341R), Anti-Caspase-3-cleaved (Cell Signaling, 9661-S), PE anti-P2ry12 (BioLegend, 848003), APC Anti-CD45 (BD Bioscience, 559864), BV421 Anti-CD11b (BD Bioscience, 562605), True Blot Anti-Rabbit Ig HRP (Rockland, 18-8816-33), and True Blot Anti-Goat Ig HRP (Rockland, 605-403-B69).

RR pharmacokinetic analysis. Vehicle control or RR treated mice (0.25mg/kg/day i.p. for 5 days) were euthanized 1h after the last injection (n=5 mice). Blood samples were collected in heparinized tubes by cardiac puncture and centrifuged (3000 g x 10 min) to obtain plasma. Brains were dissected and both plasma and brains were stored at -80ºC until bioanalysis.

RR compound levels in the plasma and brain were measured using high-performance liquid chromatography with tandem mass spectrometry (LC/MS-MS). Briefly, standards were prepared by spiking the compound in naïve mouse plasma or tissue from 0.003 – 100 nmol/mL or nmol/g. Standards, plasma (20 µL) or weighed brain samples were placed in low retention microcentrifuge tubes and extracted using methanol containing losartan as an internal standard (5 µL methanol/mg tissue). Samples were vortex mixed and centrifuged (16,000 x g for 5 minutes at 4°C). The supernatants (80 µL) were transferred to a 96 well plate and 2 µL was injected for

analysis. Samples were analyzed on an UltiMate 3000 UHPLC coupled to a Q Exactive Focus orbitrap mass spectrometer (Thermo Fisher Scientific Inc., Waltham MA). Samples were separated on an Agilent EclipsePlus C18 RRHD (1.8 µm) 2.1 × 100 mm column. The mobile phase consisted of water + 0.1% formic acid (A), and acetonitrile + 0.1% formic acid (B). Separation was achieved at a flow rate of 0.4 mL/min using a gradient run. Quantification was performed in product-reaction monitoring (PRM) mode (RR 200.1434> 145.1, 82.0650) using Xcalibur software.

Mice. Male C57BL/6J, CMV-Cre, Cx3cr1-CreER, VGlut1-Cre, VGAT-Cre, Thy1-GCaMP6s, GCaMP6s floxed, and K225A-GAPDH floxed (Zhang et al., 2022) mice were used for the experiments. All mice were on a C57BL/6 background.

K225A-GAPDH floxed model. Genetically modified mice in which lysine 225 (K) responsible for the binding between GAPDH and Siah1 was replaced with an alanine (A) residue, were generated using a homologous recombination approach (Zhang et al., 2022). In this mouse model GAPDH is not able to translocate to the nucleus, therefore the GAPDH nuclear pathway is blocked (Sen et al., 2008). These animals were crossed with Cx3cr1-CreER or CMV-Cre promoter lines in order to target microglia or blood cells respectively.

Eight to ten week old mice were used for all experiments. Mice were housed (5 mice maximum per cage) and maintained under a 12-h light: 12-h dark cycle, at a constant temperature and humidity (20–24°C, 35%–55%), with food and water available *ad libitum*. The Institutional Animal Care and Use Committee at Johns Hopkins University approved all protocols involving mice that were used in this study.

LPS and (1R, 3R)-1, 3-dimethyl-2-propargyl-1, 2, 3, 4-tetrahydroisoquinoline (RR) injections. LPS and RR were reconstituted with saline buffer. Mice were injected with saline or

RR (0.25 mg/kg/day i.p for 5 days) the day before the LPS treatment ($1.5x10^5$ EU/kg/day i.p for 4 days) started then co-treated with RR and LPS for the following 4 days.

Tamoxifen injections. The tamoxifen solution (10 mg/mL) was freshly prepared by sonicating tamoxifen freebase in sunflower seed oil (S5007, Sigma-Aldrich) at room temperature for 10–12 min (with intermittent 20 sec vortexing every 3–4 min). This solution was stored at −20°C for several months. Mice aged 4–5 weeks were administered tamoxifen by oral gavage at a dosage of 100 mg/kg body weight, once a day for two consecutive days. As microglia were the target cell, all experiments were performed five weeks after the last tamoxifen injection.

Microglia and astrocytes sorting. CD11b+ or ACSA2+ beads were used to isolate microglia or astrocytes, respectively, by magnetic sorting. The "rest" fraction corresponded with the negative fraction isolated after separating microglia and astrocytes. Microglia were isolated by fluorescence-activated cell-sorting (FACS) using CD45, CD11b, and p2ry12 antibodies (Biolegend). These cells were directly sorted into extraction lysis buffer for qPCR. RNA extraction was performed using the Arcturus Pico Pure RNA isolation kit (Thermo Fisher).

PBMC isolation. PBMCs were isolated from mouse fresh blood using a Ficoll-Paque (GE Healthcare) gradient. Blood was collected in heparin tubes, mixed 1:1 in HBSS and layered on top of an equal volume layer of Ficoll-Paque. Samples were centrifuged at 2000 rpm for 30 min at 4^oC. The layer with PBMCs was carefully extracted, diluted with PBS (1:20 dilution), and spun down to pellet the PBMCs.

Immunoblotting. PBMCs, microglia, astrocytes, or rest cells were lysed in CHAPS buffer (50 mM Tris, 150mM NaCl, 1% SDS, and 1% Triton X-100) containing a proteinase inhibitor and phosphatase inhibitor cocktails. Six rounds of sonication were performed as follows: 15 sec on, 15 sec off, and 40% amplitude with a Q125 Sonicator (Q Sonica Sonicators). Lysates were

centrifuged for 2 min at 10,000 rpm, the supernatant was collected, quantified using the Pierce BCA Protein assay (Thermo Scientific), aliquoted, and stored at -80°C until use. Lysates were thawed and 4x NuPAGE LDS sample buffer (Thermo Scientific) and 10% β-mercaptoethanol (Sigma Aldrich) were added. Lysates were heated to 95°C for 10 min and run on NuPAGE 4%–12% bis-tris gels (Invitrogen). Proteins were transferred to PVDF membranes (BioRad) and blocked for 1 hour at RT in 5% BSA in Tris buffered saline with 0.05% Tween 20 (TBST). Membranes were incubated in primary antibody overnight at 4°C, washed and incubated in secondary antibody HRP for 1 hour at RT. After washing, membranes were developed using either the Super Signal West Dura or Super Signal West Femto Chemiluminescent Substrate (Thermo Scientific).

Immunoprecipitation (IP). 200 µg of total protein was used for Siah1 IP, the total volume was increased to 1ml with supplemented CHAPS buffer, 1 µg of antibody was added and incubated O/N at 4°C with continuous agitation. For HMGB1 and HMGB2 IP, 500 µg of total protein and 2 µg of antibodies were used. On the next day cell lysates were incubated for 2h at 4°C with 30 µl of TrueBlot Anti- Goat or Rabbit Ig beads (Rockland laboratories).

Dot blot. The potency of RR and other deprenyl derivatives to block the binding between GAPDH and Siah1 was evaluated using dot blot. A mixture of GAPDH and Siah1 recombinant proteins was incubated O/N at 4°C, with each deprenyl derivative (2 nM) or deprenyl (2 nM) or empty solution. The possible protein complexes were immunoprecipitated using a Siah1 antibody as described above, and the immunoprecipitates were loaded onto a nitrocellulose membrane. The membrane was washed and immunoblotted with a GAPDH antibody as described above.

Immunohistochemistry. After perfusion, mice were fixed with 4% paraformaldehyde (PFA) and brains were kept in PFA O/N at 4°C. The following day brains were transferred to a solution of phosphate buffered saline (PBS) containing 30% sucrose for 1-2 days, then 12-30-µm cryosections were collected on glass slides. Sections were blocked in TBS containing 0.5% Triton (TBS-T) and 10% normal donkey serum (NDS) for 2 h at RT. Sections were then incubated with primary antibodies and kept at 4°C for 24-48 h. Subsequently, sections were washed three times with TBS-T for 5 min each and incubated with fluorescently conjugated-secondary antibodies for 2 h at RT. After three washes with TBS-T, sections were mounted and coverslipped. Fluorescence images were obtained using a Zeiss LSM 700, Olympus FV1000.

qRT-PCR. Total RNA from sorted cells was isolated using the ArcturusTM Pico PureTM RNA isolation kit (Thermo Fisher Scientific). Single-strand cDNA was synthesized with a High Capacity cDNA Reverse Transcription Kit (Applied Biosystems). Real-time PCR was performed using SYBR Green real-time PCR master mix (Thermo-Fisher) and a LightCycler 384 detection system (Roche).

Chromatin immunoprecipitation (ChIP). ChIP was performed as previously described (Lee et al., 2006; Nowak et al., 2005). In short, intact cells were treated with 2 mM disuccinimidyl glutarate (Pierce) to crosslink protein complexes, then treated with formaldehyde to link protein to DNA covalently. Cells were then lysed, the nucleoprotein complexes were sonicated, and the crosslinked DNA–protein complexes were enriched by IP with Acetylated (Lysine-160)-GAPDH antibody (Millipore Sigma) or Rabbit IgG (Invitrogen).

ChIP-Seq. DNA libraries were generated using the DNA SMART^{TM} ChIP-Seq Kit (Clontech) and sequenced using paired end HiSeq2500 (Illumina). FastQC was used to quality control sequencing reads. The reads were aligned to the mm10 genome with bowtie2. Peak finding was

performed by MACS1.4 with default parameters. Peak annotation was performed with Peak Annotation and Visualization (https://manticore.niehs.nih.gov/pavis2/).

Motif analysis. Motif enrichment and discovery analysis were performed using CentriMO and MEME-ChIP software using default parameters (Ma et al., 2014).

Ingenuity Pathway Analysis. Ingenuity Pathway Analysis software (Ingenuity Systems, CA) was used to investigate interactions between the genes targeted by N-GAPDH. Interactive pathways were generated to observe potential direct and indirect relations among these genes. To test the possibly enriched pathways targeted by N-GAPDH we considered direct and indirect relationships that were experimentally observed.

Acute brain slice preparation. Mice were anesthetized with ether, perfused using cold N-methyl-D-glucamine (NMDG) based cutting solution containing (in mM): 135 NMDG, 1 KCl, 1.2 KH_2PO_4, 1.5 $MgCl_2$, 0.5 $CaCl_2$, 10 Dextrose, 20 Choline Bicarbonate, (pH 7.4) as previously described (*94*). Brains were dissected and mounted on a vibratome (Leica VT100S). Cortical slices 250 μm thick were cut in ice-cold N-methyl-D-glucamine (NMDG) based cutting solution. Cortical slices were then transferred to artificial cerebral spinal fluid (ACSF) containing (in mM): 119 NaCl, 2.5 KCl, 2.5 $CaCl_2$, 1.3 $MgCl_2$, 1 NaH_2PO_4, 26.2 $NaHCO_3$, and 11 Dextrose (292–298 mOsm/L) and were maintained at 37° C for 40 min, and at room temperature thereafter. Both the NMDG solution and ACSF were bubbled continuously with 95% O_2/5% CO_2. All slice imaging experiments were carried out at room temperature. Acute treatment of LSM slices with a solution of anti-HMGB1 antibody in ACSF (1:50 dilution) was performed for the LSM + HMGB1 Ab condition.

Ca imaging recording and analysis. Fluorescence dynamics arising from GCaMP6s VGlut1, VGAT, or Thy1 positive neurons were recorded using a fixed-stage microscope (BX61-WI,

Olympus) with optical lens (40x-0.80, LumPLanFL N), 300 W Xenon lamp using a GFP filter, high speed galvo mirror with filters (DG4-1015, Shutter Instrument Company), and an infrared-sensitive CCD camera (iXon3, ANDOR Technology). Images were processed with digital imaging software (MetaFluor® for Olympus and Metamorph Advanced Molecular Device). All these systems were on an anti-vibration floating table (Technical Management Corp.) and connected to a PC (Windows 7, Microsoft). For imaging analysis, raw videos were pre-processed by applying ×4 spatial down-sampling to reduce file size and processing time, but no temporal down-sampling was applied (Zhou et al., 2018). To reliably deal with the large fluctuating background, we applied the CNMFe algorithm that is a recent adaptation of the CNMF algorithm (Pnevmatikakis et al., 2016), enabling us to identify individual neurons, obtain their fluorescent traces, and deconvolve fluorescence signals into neural activity. To define the initial spatial components, candidate seed pixels were manually selected from peak-to-noise (PNR) graphs of the field of view (FOV) (Murugan et al., 2017). Calcium events with z-scores < 8 or those that did not have a >0.5 AUC were excluded from analyses because events of this magnitude did not reliably retain transient, calcium-event characteristics across animals.

Slice electrophysiology recordings. Mice were deeply anesthetized with isoflurane. Animals irresponsive to toe pinches were decapitated, and brains were rapidly extracted and sliced using a vibratome (Leica VT-1200). The cutting solution contained (in mM) 85 NaCl, 65 sucrose, 25 $NaHCO_3$, 10 glucose, 4 $MgCl_2$, 2.5 KCl, 1.25 NaH_2PO_4, 0.5 $CaCl_2$ (pH 7.35, ~308 mOsm). 300 μm slices containing the prelimbic cortex were collected and recovered for 10 min in the same cutting solution at 32°C, then slices were transferred to ACSF solution containing (in mM) 130 NaCl, 24 $NaHCO_3$, 10 glucose, 3.5 KCl, 2.5 $CaCl_2$, 1.5 $MgSO_4$, 1.25 NaH_2PO_4 (pH 7.35, ~303 mOsm). Slices were left to recover for 1h at room temperature before recordings. All ACSF

solutions were saturated with 95% O_2 and 5% CO_2. For recording, a single slice was transferred to a heated chamber (34-35°C) and perfused with ACSF using a peristaltic pump (WPI). GCaMP6s-expressing excitatory neurons in Layer 5 in the prelimbic cortex were identified on an upright microscope equipped for differential interference contrast (DIC) microscopy (Olympus BX51WI) and LED fluorescence (X-Cite, 120 LED). Whole-cell patch-clamp recordings were made using a MultiClamp 700B amplifier (1 kHz low-pass Bessel filter and 10 kHz digitization) with pClamp 10.3 software (Molecular Devices). Voltage-clamp recordings were made using borosilicate glass pipets (King Precision Glass Inc., KG-33 ID 1.00 OD 1.50) with resistance 1.5-3.0 MΩ, filled with internal solution containing (in mM): 117 Cs-methanesulphonate, 20 HEPES, 5 QX-314, 5 TEA-Cl, 4 ATP-Mg, 2.8 NaCl, 1 Na_2-phosphocreatine, 0.4 EGTA, 0.4 GTP-Na (pH 7.30, ~290 mOsm). Access resistance was continually monitored throughout recording; cells in which access resistance rose above 20 MΩ were excluded from analysis. Membrane potentials were not corrected for junction potentials. Electrical stimuli were delivered using a bipolar stimulating electrode (FHC, MX21AES) placed medial to the recorded cell, in the presence of SR-95531 (GABAa receptor antagonist) (5 μM) and DNQX (AMPA receptor antagonist) (10 μM) to isolate NMDA receptor-mediated currents, which were verified by adding AP5 (50 μM) at the end of recordings. Analysis was performed offline using Clampfit (v 10.6).

Cognitive flexibility tasks. We followed a protocol described by Cho *et al* (Cho et al., 2015) with some adaptations from Heisler *et al* (Heisler et al., 2015). Briefly, mice were single-housed and habituated to a reverse light/dark cycle at least two weeks before starting the task. Food intake was restricted 5 days before starting, corresponding to the period in which the mice were adapted to the bowls and reward. At the start of each trial, the mouse was placed in its home cage to explore two bowls, each containing one odor and one digging medium, until it dug in one

bowl, signifying a choice. The bait was a piece of a peanut butter chip (approximately 5-10 mg in weight) and the cues, either olfactory (odor) or somatosensory and visual (texture of the digging medium which hides the bait), were altered and counterbalanced. All cues were presented in small animal food bowls (All Living Things Nibble bowls, PetSmart) that were identical in color and size. Digging media was mixed with the odor (0.1% by volume) and peanut butter chip powder (0.1% by volume). All odors were ground dried spices (McCormick garlic and coriander). Unscented digging media was purchased from Cole Hardware and Cole Valley Pets (Mosser Lee white sand, litter). For each trial, while the odor-medium combination present in each of the two bowls may have changed, the stimulus (e.g., a particular odor or medium) that signaled the presence of the food reward remained constant over each portion of the task (initial association, rule shift). If the initial association paired a specific odor with the food reward, then the digging medium would be considered the irrelevant dimension. The mouse was considered to have learned the initial association between stimulus and reward if it made 8 correct choices during 10 consecutive trials. Each portion of the task ended when the mouse met this criterion. Following the initial association, the rule-shifting portion of the task began, and the stimulus associated with the reward underwent an extra-dimensional shift. For example, if an odor had been associated with the reward during the initial association, then a digging medium was associated with the reward during the rule-shifting portion of the task. The mouse was considered to have learned this extra dimensional rule shift if it made 8 correct choices during 10 consecutive trials. In all portions of the task, after the mouse made an error on a trial or 3 min passed with no choice, the mouse was transferred to the holding (punishment) cage for a minimum of 60 sec. If the animal made 6 consecutive no choices (3 min without a choice) this was recorded as a failure to participate.

Forced swim test. Each mouse was put in Plexiglass cylinder tanks measuring 19 cm in height and 13 cm in diameter with a water level of 16 cm. Mice were scored for immobility time over a 6-min uninterrupted test session.

Open field test. An individual mouse was placed near the wall-side of a 50 x 50 cm open-field arena. The movement of the mouse was recorded by laser beam breaks for 30 min using an infrared activity monitor (San Diego Instruments). The data was automatically analyzed with PAS-Open Field software (San Diego Instruments). Time in the center of the field and total activity were measured. The open field arena was cleaned with 70% ethanol and wiped with paper towels between each trial.

The Institutional Animal Care and Use Committee at Johns Hopkins University approved all protocols used in this study.

Human cells: Chronic schizophrenia patients and subjects with first episode psychosis were recruited at the Johns Hopkins Schizophrenia Center and Zucker Hillside Hospital. Age-, gender-, and race-matched controls were recruited at each site. This study was approved by the Johns Hopkins School of Medicine Institutional Review Board (NA_00037204) and the Zucker Hillside Hospital Institutional Review Board (NCT00320671).

PBMC isolation and lymphoblast generation. PBMCs were isolated from patient blood using a Ficoll-Plaque gradient. Blood was collected in heparin tubes, mixed 1:1 in HBSS and layered on top of an equal volume layer of Ficoll-Paque. Samples were centrifuged at 2000 rpm for 30 min at 4°C. The layer with PBMCs was carefully extracted, diluted with PBS (1:20 dilution), and spun down to pellet the PBMCs. Lymphoblasts were prepared from PBMCs as previously described (Bader et al., 2012).

Clinical and cognitive assessment. The Evaluation of Psychiatric symptoms was performed using the Scales for the Assessment of Positive Symptoms (SAPS) and the Assessment of Negative Symptoms (SANS). In regard to neurocognitive evaluations, a battery of neuropsychological tests which covered 6 cognitive domains was used (Horiuchi et al., 2016).

Quantifications and statistical analysis:

Animal data. All data are expressed as the mean ± SEM. Quantification of confocal microscopy, immunoblots, Ca^{2+} imaging, and slice electrophysiology recordings was performed using Imaris, ImageJ, MATLAB, and Clampfit respectively. Statistical differences between two groups were determined by a two-tailed unpaired Student's *t*-test. For multiple group datasets, two-way or one-way ANOVA analysis was used, followed by Tukey's multiple comparisons test for more than two groups. For multiple group datasets of slice electrophysiology recordings, repeated measures ANOVA analysis was used, followed by Dunnett's post-hoc tests. Statistical tests used to measure significance are indicated in each figure legend along with the corresponding significance level (p value).

Human data. Multiple linear regression analyses were employed to examine whether cellular AF levels can predict performance in a specific cognitive function(s) after controlling for age, gender, race, and smoking status. Missing values for cognitive performance were imputed using the R missForest function. Multiple linear regression analyses were performed with the original and the imputed values. The effect of medication on AF was addressed by introducing a cohort of first episode of psychosis patients; changes in the levels of AF before and after antipsychotic medication were addressed using two-tailed paired t-tests. The relationship between AF and HMGB1 and HMGB2 expression levels were examined by Spearman correlation.

ACKNOWLEDGEMENTS

We appreciate Melissa A. Landek-Salgado for thoughtful comments and editions of this manuscript. We also thank Yukiko Lema for figure and manuscript organization. We would like to thank Hao Zhang and the Flow Cytometry Core at JHSPH for providing sorting and analysis services. We appreciate Liliana Florea and Corina Antonescu at JHMI for providing whole genome sequencing analysis services. We thank Francisco Dominguez for technical support.

Funding: This work was supported by the grants from the National Institute of Health (MH-094268 Silvio O. Conte center, MH-105660, MH-107730), as well as the grants from NARSAD, Stanley, and S-R/RUSK (all to A.S.).

AUTHOR CONTRIBUTIONS

A.R., K.I., H.N., L.N.H., A.Saito, A.Sengupta, R.S., C.C., A.H., N.E., T.P., E.C., T.T., M.N., S.I., and E.T. performed and also contributed to experiments by guiding the use of reagents and animals for the study. R.R., B.S., and T.S. performed pharmacokinetic analysis and also contributed to experiments by guiding the use of the chemicals synthesized in the lab of T.S.. D.R., J.G., and A.M. provided human samples and contributed to the discussion. A.S and A.R. designed the experiments. A.S., A.R., and K.I. contributed to writing the manuscript. A.S. supervised the research.

DECLARATION OF INTERESTS

The authors declare no competing interests.

FIGURE LEGENDS

Figure 1. The N-GAPDH cascade underlies cognitive flexibility in a stress-induced mouse model.

(A) Schematic diagram of the mouse paradigm and behavioral task. Eight to ten week-old mice were adapted to a reverse light/dark cycle. Drug injections were made intraperitoneally (ip). Mice were food restricted for 72 h before starting habituation, then habituated for 2 consecutive days to the bowls, digging media, and food reward before testing began. Mice that reached criteria were tested with the behavioral task on the following day. Black arrowhead, injection; red line, calorie restriction; yellow arrowhead, habituation; and brown arrowhead, behavioral test.

(B) Schematic diagram illustrating the rule-shifting task. Two bowls were presented to mice, each baited by an odor (O1 or O2) and a textured digging medium (TA or TB). Mice had to find a food reward that was associated with a particular stimulus (indicated in red) buried in the digging medium. Mice first learned an initial association; once mice reached the learning criterion (eight correct out of ten consecutive trials), this association underwent an extra-dimensional rule shift.

(C) Performance of Control, RR, LSM, and RR LSM mice in the rule shifting task. Each dot represents data from an individual mouse. Two-way ANOVA (RR x LSM) revealed a significant main effect of RR ($F_{(1,37)} = 4.68$, $p=0.037$), a significant effect of LSM ($F_{(1,37)} = 7.33$, $p =0.010$), and a non-significant interaction between factors ($F_{(1,37)} = 2.55$, $p=0.119$). Error bars represent the mean ± SEM. $^{\#}p =0.051$ $^{*}p <0.05$ by two-way ANOVA with Tukey's multiple comparisons test.

(D) LSM mice performed significantly more perseverant than random errors during the rule-shifting task. Each dot represents data from an individual mouse. Two-way ANOVA (RR x LSM) revealed a significant main effect of RR ($F_{(1,37)} = 6.66$, $p=0.014$), a significant effect of LSM ($F_{(1,37)} = 7$, $p=0.012$), and a non-significant interaction between factors ($F_{(1,37)} = 3.12$, $p=0.086$). Error bars represent the mean ± SEM. *$p < 0.05$, **$p < 0.01$ by two-way ANOVA with Tukey's multiple comparisons test.

Figure 2. Stress induced upregulation of the N-GAPDH cascade selectively in microglia.

(A) Schematic diagram showing the mouse intraperitoneal injection paradigm used.

(B) Levels of GAPDH-Siah1 binding (a key indicator of the N-GAPDH cascade activation). Lysates were from cortical microglia and astrocytes isolated from Control and LSM mice using magnetic sorting. "Rest" corresponds to the negative fraction after isolation of microglia and astrocytes. The purity of isolated cells was assessed by using anti-Iba1, NeuN, and Aldh1L1 antibodies that specifically recognize microglia, neurons, and astrocytes, respectively. The Y axis depicts the level of GAPDH-Siah1 binding, which was normalized by the level of Siah1.

(C) Representative confocal images depicting sulfonated GAPDH at cysteine-150 (SulfoGAPDH) co-localized with microglia (Iba1), and not astrocytes (GFAP) or neural cells (NeuN), in LSM mice. Arrows indicate Iba1 and SulfoGAPDH signals, whereas arrowheads indicate colocalization of the Iba1 and SulfoGAPDH signals. Scale bar: 40 μm.

(D) Level of GAPDH-Siah1 binding. Lysates were from cortical and striatal microglia isolated from Control and LSM mice. The Y axis depicts the level of GAPDH-Siah1 binding, which was normalized by the level of Siah1.

(E) Level of GAPDH-Siah1 binding. Lysates were from cortical microglia isolated from Control, LSM, and RR LSM mice. The Y axis depicts the level of GAPDH-Siah1 binding, which was normalized by the level of Siah1.

(F) Performance of Control, LSM, and K225A-MG LSM mice in the rule shifting task. Each dot represents data from an individual mouse.

(G) LSM mice performed significantly more perseverant than random errors during the rule-shifting task. Each dot represents data from an individual mouse.

Error bars represent the mean ± SEM. *$p < 0.05$, **$p < 0.01$ by unpaired two-tailed t-test for panels (B) and (D), and one-way ANOVA with Tukey's multiple comparisons test for panels (E), (F), and (G). Immunoblots are representative of 5 independent experiments from cells isolated from 10 mice per group [(B), (D), and (E)]. Confocal images are representative of 3 mice per group (C).

Figure 3. Whole-genome landscape of transcriptional regulation by N-GAPDH in stressed microglia.

(A) Schematic diagram of the chromatin immunoprecipitation (ChIP) approach used to specifically target N-GAPDH, with an antibody against acetylated GAPDH at Lys-160, in cortical microglia isolated from LSM mice.

(B**)** Pie graph showing the distribution of chromatin occupancy peaks.

(C) The top 5 representative motif sequences for the N-GAPDH ChIP-ed regions identified using CentriMo motif enrichment analysis. The estimated statistical significance of the discovered motifs is expressed using p and E values derived from a one-tailed binomial test. Enrichment E-values were computed by first adjusting the binomial p-value of a region for the number of

regions tested using the Bonferroni correction, and then multiplying the adjusted p-value by the number of motifs in the input to CentriMo.

(D) The top 5 representative de novo motif sequences for the N-GAPDH ChIP-ed regions identified using MEME-ChIP motif discovery analysis. Statistical significance of a motif is reported as an E-value.

(E) The top 5 canonical pathways depicted by Ingenuity Pathway Analysis.

Figure 4. The N-GAPDH cascade regulates HMGB signaling in microglia.

(A) Schematic diagram from the Integrative Genomics Viewer (IGV) representing N-GAPDH occupancy on the promoter region of *Hmgb2*. The Model-based Analysis of ChIP-Seq (MACS) algorithm called 721 peaks of N-GAPDH occupancy, among them MACS_Peak_649 was on the promoter region of *Hmgb2*.

(B) ChIP-qPCR data confirmed binding of the protein complex that included N-GAPDH to the Hmgb2 promoter region. Microglia from Control, LSM, and RR LSM mice were tested. Rabbit IgG immunoprecipitations were used as a negative control in LSM microglia. Three experiments were performed with cortical microglia isolated from 15 mice per group.

(C) Level of HMGB2 mRNA in microglia from Control, LSM, RR LSM, and K225A-MG LSM [Cx3cr1-CreER;K225A-GAPDH LSM] mice. Each dot represents data from an individual mouse.

(D) Level of HMGB1 and HMGB2 protein in microglia from Control, LSM, RR LSM, and K225A-MG LSM mice The Y axis depicts the level of HMGB1 and HMGB2, which were normalized by the level of H3. Immunoblots are representative of 6 independent experiments from cortical microglia isolated from 5 mice per group.

(E) Quantification of lysosomal HMGB1 and HMGB2 using volumetric analysis of 3D microglia stack reconstructions from Control, LSM, and RR LSM mice. Microglia and lysosomes were stained with an antibody against Iba1 and CD68, respectively. Analysis was performed using Imaris as previously described. Scale bar: 10 μm. Confocal images are representative of 8 z-stack images from 2 mice per group.

Error bars represent mean ± SEM. *$p < 0.05$, **$p < 0.01$, ***$p<0.001$ by one-way ANOVA with Tukey's multiple comparisons test.

Figure 5. Microglial HMGB proteins modulate neural activity in prelimbic pyramidal neurons without causing excitotoxicity.

(A) A representative image of a brain slice from a LSM mouse showing expression of VGlut1 neuron specific promoter-driven GCaMP6s in prelimbic cortical neurons (left) and time courses of the fluorescence change ($\Delta F/F$) in the 9 neurons labeled 1-9 in the left panel (right). Brain slices were recorded at basal level and no stimulation was performed.

(B) Frequency (left) and peak amplitude (right) for 47 VGlut1-positive cells from 4 Control mice, 57 VGlut1-positive cells from 4 LSM mice, 89 VGlut1-positive cells from 4 RR LSM mice, and 111 VGlut1-positive cells from 4 LSM mice acutely treated with an antibody against HMGB1. **$p < 0.01$, ***$p<0.001$ by one-way ANOVA with Tukey's multiple comparisons test.

(C) Frequency (left) and peak amplitude (right) for 68 VGlut1-positive cells from 3 Control mice, 238 VGlut1-positive cells from 3 LSM mice, and 171 VGlut1-positive cells from 3 K225A-MG LSM mice. ***$p<0.001$ by one-way ANOVA with Tukey's multiple comparisons test.

(D) Frequency (left) and peak amplitude (right) for 169 VGAT-positive cells from 3 Control mice, and 119 VGAT-positive cells from 5 LSM mice. No statistical difference was detected by a two-tailed unpaired Student's *t*-test.

(E) Representative traces (top) of electrically evoked NMDA receptor-mediated currents recorded from GCaMP6s-expressing layer 5 excitatory neurons in the prelimbic area at different holding potentials in acute brain slices (+35mV, +15mV, −5mV, −25mV, −45mV, −65mV, and −85mV). A graph (bottom) shows average normalized current-voltage relationships (7 cells from 3 Control mice, 8 cells from 4 LSM mice, 7 cells from 3 K225A-MG LSM mice). *$p < 0.05$, **$p<0.01$ by repeated measures ANOVA with Dunnett's post-hoc test.

For each panel, error bars represent the mean ± SEM.

Figure 6. Peripheral N-GAPDH cascade related pathology in the LSM model.

(A) Immunoblots for HMGB1 and HMGB2 using PBMC lysates from Control [CMV-Cre;WT-GAPDH], LSM [CMV-Cre;WT-GAPDH LSM], and K225A-Pan LSM [CMV-Cre;K225A-GAPDH LSM] mice. The Y axis depicts the level of HMGB1 and HMGB2, which were normalized by the level of tubulin.

(B) Autofluorescence (AF) levels in PBMCs from Control, LSM, and K225A-Pan LSM mice were measured by flow cytometry using the FL1 channel. Each dot represents data from an individual mouse.

(C) Levels of GAPDH-Siah1 binding in PBMCs from LSM and K225A-Pan LSM mice. The Y axis depicts the level of GAPDH-Siah1 binding, which was normalized by the level of Siah1. Error bars represent the mean ± SEM. *$p < 0.05$, **$p < 0.01$ by one-way ANOVA with Tukey's multiple comparisons test for panels (A) and (B), and unpaired two tailed t test for panel (C).

Immunoblots are representative of 4 independent experiments from PBMCs isolated from 5 mice per group [(A) and (C)].

Figure 7. AF levels in lymphoblasts in correlation with cognitive flexibility: A human clinical study.

(A) Demographic data for the clinical cohort that includes healthy controls and patients with schizophrenia (SZ). AA, African American; Cauc, Caucasian; Other, Non-AA and Non-Cauc.

(B) Association between executive function and autofluorescence (AF) shown in a multiple linear regression model. Data are adjusted for major confounding factors, such as age, gender, race, and smoking status. Executive function was assessed by the Wisconsin Card Sorting Test (WCST).

(C) Graphical representation of the unadjusted association between AF levels in lymphoblasts and executive function represented as the WCST score.

(D) Antipsychotic medication does not influence AF, assessed by a paired two-tailed t-test.

(E) Spearman correlation of AF levels with HMGB1 protein levels in lymphoblasts from SZ patients and control subjects. R=0.46, p=0.020.

REFERENCES

Agarwal, A., Wu, P.H., Hughes, E.G., Fukaya, M., Tischfield, M.A., Langseth, A.J., Wirtz, D., and Bergles, D.E. (2017). Transient Opening of the Mitochondrial Permeability Transition Pore Induces Microdomain Calcium Transients in Astrocyte Processes. Neuron *93*, 587–605.e7.

Arnsten, A.F.T. (2009). Stress signalling pathways that impair prefrontal cortex structure and function. Nat. Rev. Neurosci. *10*, 410–422.

Bader, V., Tomppo, L., Trossbach, S. V., Bradshaw, N.J., Prikulis, I., Rutger Leliveld, S., Lin, C.Y., Ishizuka, K., Sawa, A., Ramos, A., et al. (2012). Proteomic, genomic and translational approaches identify CRMP1 for a role in schizophrenia and its underlying traits. Hum. Mol. Genet. *21*, 4406–4418.

Balch, W.E., Morimoto, R.I., Dillin, A., and Kelly, J.W. (2008). Adapting proteostasis for disease intervention. Science. *319*, 916–919.

Barreiro-Alonso, A., Lamas-Maceiras, M., Rodríguez-Belmonte, E., Vizoso-Vázquez, Á., Quindós, M., and Cerdán, M.E. (2016). High Mobility Group B Proteins, Their Partners, and Other Redox Sensors in Ovarian and Prostate Cancer. Oxid. Med. Cell. Longev. *2016*.

Barreiro-Alonso, A., Cámara-Quílez, M., Salamini-Montemurri, M., Lamas-Maceiras, M., Vizoso-Vázquez, Á., Rodríguez-Belmonte, E., Quindós-Varela, M., Martínez-Iglesias, O., Figueroa, A., and Cerdán, M.E. (2019). Characterization of HMGB1/2 interactome in prostate

cancer by yeast two hybrid approach: Potential pathobiological implications. Cancers (Basel). *11*.

Baudic, S., Barba, G.D., Thibaudet, M.C., Smagghe, A., Remy, P., and Traykov, L. (2006). Executive function deficits in early Alzheimer's disease and their relations with episodic memory. Arch. Clin. Neuropsychol. *21*, 15–21.

Berman, K.F., Zec, R., and Weinberger, D.R. (1985). Physiological dysfunction of dorsolateral prefrontal cortex in schizophrenia. Fed. Proc. *44*.

Bissonette, G.B., Martins, G.J., Franz, T.M., Harper, E.S., Schoenbaum, G., and Powell, E.M. (2008). Double dissociation of the effects of medial and orbital prefrontal cortical lesions on attentional and affective shifts in mice. J. Neurosci. *28*, 11124–11130.

Boukouris, A.E., Zervopoulos, S.D., and Michelakis, E.D. (2016). Metabolic Enzymes Moonlighting in the Nucleus: Metabolic Regulation of Gene Transcription. Trends Biochem. Sci. *41*, 712–730.

Buttgereit, A., Lelios, I., Yu, X., Vrohlings, M., Krakoski, N.R., Gautier, E.L., Nishinakamura, R., Becher, B., and Greter, M. (2016). Sall1 is a transcriptional regulator defining microglia identity and function. Nat. Immunol. *17*, 1397–1406.

Bygrave, A.M., Kilonzo, K., Kullmann, D.M., Bannerman, D.M., and Kätzel, D. (2019). Can N-

Methyl-D-Aspartate Receptor Hypofunction in Schizophrenia Be Localized to an Individual Cell Type? Front. Psychiatry *10*.

Callicott, J.H. (2000). Physiological Dysfunction of the Dorsolateral Prefrontal Cortex in Schizophrenia Revisited. Cereb. Cortex *10*, 1078–1092.

Carlén, M., Meletis, K., Siegle, J.H., Cardin, J.A., Futai, K., Vierling-Claassen, D., Rühlmann, C., Jones, S.R., Deisseroth, K., Sheng, M., et al. (2012). A critical role for NMDA receptors in parvalbumin interneurons for gamma rhythm induction and behavior. Mol. Psychiatry *17*, 537–548.

Chang, C.H., Curtis, J.D., Maggi, L.B., Faubert, B., Villarino, A. V., O'Sullivan, D., Huang, S.C.C., Van Der Windt, G.J.W., Blagih, J., Qiu, J., et al. (2013). XPosttranscriptional control of T cell effector function by aerobic glycolysis. Cell *153*, 1239.

Cheng, S.C., Quintin, J., Cramer, R.A., Shepardson, K.M., Saeed, S., Kumar, V., Giamarellos-Bourboulis, E.J., Martens, J.H.A., Rao, N.A., Aghajanirefah, A., et al. (2014). MTOR- and HIF-1α-mediated aerobic glycolysis as metabolic basis for trained immunity. Science (80-.). *345*.

Cho, K.K.A., Hoch, R., Lee, A.T., Patel, T., Rubenstein, J.L.R., and Sohal, V.S. (2015). Gamma rhythms link prefrontal interneuron dysfunction with cognitive inflexibility in dlx5/6+/- mice. Neuron *85*, 1332–1343.

Cissé, M., Halabisky, B., Harris, J., Devidze, N., Dubal, D.B., Sun, B., Orr, A., Lotz, G., Kim, D.H., Hamto, P., et al. (2011). Reversing EphB2 depletion rescues cognitive functions in Alzheimer model. Nature *469*, 47–52.

Colell, A., Green, D.R., and Ricci, J.E. (2009). Novel roles for GAPDH in cell death and carcinogenesis. Cell Death Differ. *16*, 1573–1581.

Colombo, E., and Farina, C. (2016). Astrocytes: Key Regulators of Neuroinflammation. Trends Immunol. *37*, 608–620.

Colonna, M., and Butovsky, O. (2017). Microglia Function in the Central Nervous System During Health and Neurodegeneration. Annu. Rev. Immunol. *35*, 441–468.

Coughlin, J.M., Ishizuka, K., Kano, S.I., Edwards, J.A., Seifuddin, F.T., Shimano, M.A., Daley, E.L., Zandi, P.P., Leweke, F.M., Cascella, N.G., et al. (2013). Marked reduction of soluble superoxide dismutase-1 (SOD1) in cerebrospinal fluid of patients with recent-onset schizophrenia. Mol. Psychiatry *18*, 10–11.

Coughlin, J.M., Hayes, L.N., Tanaka, T., Xiao, M., Yolken, R.H., Worley, P., Leweke, F.M., and Sawa, A. (2017). Reduced superoxide dismutase-1 (SOD1) in cerebrospinal fluid of patients with early psychosis in association with clinical features. Schizophr. Res. *183*, 64–69.

Dantzer, R., O'Connor, J.C., Freund, G.G., Johnson, R.W., and Kelley, K.W. (2008). From

inflammation to sickness and depression: When the immune system subjugates the brain. Nat. Rev. Neurosci. *9*, 46–56.

Diamond, A. (2013). Executive Functions Adele. Annu. Rev. Psychol. *24*, 135–168.

Floresco, S.B., Zhang, Y., and Enomoto, T. (2009). Neural circuits subserving behavioral flexibility and their relevance to schizophrenia. Behav. Brain Res. *204*, 396–409.

Fu, L., Liu, K., Wake, H., Teshigawara, K., Yoshino, T., Takahashi, H., Mori, S., and Nishibori, M. (2017). Therapeutic effects of anti-HMGB1 monoclonal antibody on pilocarpine-induced status epilepticus in mice. Sci. Rep. *7*.

Gardella, S., Andrei, C., Ferrera, D., Lotti, L. V., Torrisi, M.R., Bianchi, M.E., and Rubartelli, A. (2002). The nuclear protein HMGB1 is secreted by monocytes via a non-classical, vesicle-mediated secretory pathway. EMBO Rep. *3*, 995–1001.

Glass, C.K., Saijo, K., Winner, B., Marchetto, M.C., and Gage, F.H. (2010). Mechanisms Underlying Inflammation in Neurodegeneration. Cell *140*, 918–934.

Gruber, A.J., Calhoon, G.G., Shusterman, I., Schoenbaum, G., Roesch, M.R., and O'Donnell, P. (2010). More is less: A disinhibited prefrontal cortex impairs cognitive flexibility. J. Neurosci. *30*, 17102–17110.

Guha, P., Harraz, M.M., and Snyder, S.H. (2016). Cocaine elicits autophagic cytotoxicity via a

nitric oxide-GAPDH signaling cascade. Proc. Natl. Acad. Sci. U. S. A. *113*, 1417–1422.

Hammond, T.R., Marsh, S.E., and Stevens, B. (2019). Immune Signaling in Neurodegeneration. Immunity *50*, 955–974.

Hampel, H., O'Bryant, S.E., Molinuevo, J.L., Zetterberg, H., Masters, C.L., Lista, S., Kiddle, S.J., Batrla, R., and Blennow, K. (2018). Blood-based biomarkers for Alzheimer disease: mapping the road to the clinic. Nat. Rev. Neurol. *14*, 639–652.

Hancock, E.J., Ang, J., Papachristodoulou, A., and Stan, G.B. (2017). The Interplay between Feedback and Buffering in Cellular Homeostasis. Cell Syst. *5*, 498–508.e23.

Hara, M.R., Agrawal, N., Kim, S.F., Cascio, M.B., Fujimuro, M., Ozeki, Y., Takahashi, M., Cheah, J.H., Tankou, S.K., Hester, L.D., et al. (2005). S-nitrosylated GAPDH initiates apoptotic cell death by nuclear translocation following Siah1 binding. Nat. Cell Biol. *7*, 665–674.

Hara, M.R., Thomas, B., Cascio, M.B., Bae, B. Il, Hester, L.D., Dawson, V.L., Dawson, T.M., Sawa, A., and Snyder, S.H. (2006). Neuroprotection by pharmacologic blockade of the GAPDH death cascade. Proc. Natl. Acad. Sci. U. S. A. *103*, 3887–3889.

Hayes, L.N., Severance, E.G., Leek, J.T., Gressitt, K.L., Rohleder, C., Coughlin, J.M., Leweke, F.M., Yolken, R.H., and Sawa, A. (2014). Inflammatory molecular signature associated with infectious agents in psychosis. Schizophr. Bull. *40*, 963–972.

He, S.J., Cheng, J., Feng, X., Yu, Y., Tian, L., and Huang, Q. (2017). The dual role and therapeutic potential of high-mobility group box 1 in cancer. Oncotarget *8*, 64534–64550.

Heisler, J.M., Morales, J., Donegan, J.J., Jett, J.D., Redus, L., and O'connor, J.C. (2015). The attentional set shifting task: A measure of cognitive flexibility in mice. J. Vis. Exp.

Horiuchi, Y., Kondo, M.A., Okada, K., Takayanagi, Y., Tanaka, T., Ho, T., Varvaris, M., Tajinda, K., Hiyama, H., Ni, K., et al. (2016). Molecular signatures associated with cognitive deficits in schizophrenia: a study of biopsied olfactory neural epithelium. Transl. Psychiatry *6*, e915.

Ihle, J.N. (1996). STATs: Signal transducers and activators of transcription. Cell *84*, 331–334.

Ionescu, T. (2012). Exploring the nature of cognitive flexibility. New Ideas Psychol. *30*, 190–200.

Jackson, M.E., Homayoun, H., and Moghaddam, B. (2004). NMDA receptor hypofunction produces concomitant firing rate potentiation burst activity reduction in the prefrontal cortex. Proc. Natl. Acad. Sci. U. S. A. *101*, 8467–8472.

Johnson, A.W., Jaaro-Peled, H., Shahani, N., Sedlak, T.W., Zoubovsky, S., Burruss, D., Emiliani, F., Sawa, A., and Gallagher, M. (2013). Cognitive and motivational deficits together with prefrontal oxidative stress in a mouse model for neuropsychiatric illness. Proc. Natl. Acad.

Sci. U. S. A. *110*, 12462–12467.

Jones, R.W. (1965). Homeostasis and Feedback Mechanisms . G. M. Hughes . Q. Rev. Biol. *40*, 395–395.

Kim, I.D., Lee, H., Kim, S.W., Lee, H.K., Choi, J., Han, P.L., and Lee, J.K. (2018). Alarmin HMGB1 induces systemic and brain inflammatory exacerbation in post-stroke infection rat model. Cell Death Dis. *9*.

Kim, J. Bin, Joon, S.C., Yu, Y.M., Nam, K., Piao, C.S., Kim, S.W., Lee, M.H., Han, P.L., Park, J.S., and Lee, J.K. (2006). HMGB1, a novel cytokine-like mediator linking acute neuronal death and delayed neuroinflammation in the postischemic brain. J. Neurosci. *26*, 6413–6421.

Kirkpatrick, B., Miller, B., García-Rizo, C., and Fernandez-Egea, E. (2014). Schizophrenia: A systemic disorder. Clin. Schizophr. Relat. Psychoses *8*, 73–79.

Krance, S.H., Wu, C.Y., Zou, Y., Mao, H., Toufighi, S., He, X., Pakosh, M., and Swardfager, W. (2019). The complement cascade in Alzheimer's disease: a systematic review and meta-analysis. Mol. Psychiatry.

Landek-Salgado, M.A., Faust, T.E., and Sawa, A. (2016). Molecular substrates of schizophrenia: Homeostatic signaling to connectivity. Mol. Psychiatry *21*, 10–28.

Lee, S., Nam, Y., Koo, J.Y. oun., Lim, D., Park, J., Ock, J., Kim, J., Suk, K., and Park, S.B. u.

(2014). A small molecule binding HMGB1 and HMGB2 inhibits microglia-mediated neuroinflammation. Nat. Chem. Biol. *10*, 1055–1060.

Lee, T.I., Johnstone, S.E., and Young, R.A. (2006). Chromatin immunoprecipitation and microarray-based analysis of protein location. Nat. Protoc. *1*, 729–748.

Ma, W., Noble, W.S., and Bailey, T.L. (2014). Motif-based analysis of large nucleotide data sets using MEME-ChIP. Nat. Protoc. *9*, 1428–1450.

Malloy, P., and McLaughlin, N.C.R. (2010). Everyday functioning in dementia and mild cognitive impairment. Neuropsychol. Everyday Funct. 264–279.

Marshall, G.A., Rentz, D.M., Frey, M.T., Locascio, J.J., Johnson, K.A., and Sperling, R.A. (2011). Executive function and instrumental activities of daily living in MCI and AD. Alzheimer's Dement. *7*, 300–308.

Moghaddam, B., and Javitt, D. (2012). From revolution to evolution: The glutamate hypothesis of schizophrenia and its implication for treatment. Neuropsychopharmacology *37*, 4–15.

Moghaddam, B., and Krystal, J.H. (2012). Capturing the angel in angel dust: Twenty years of translational neuroscience studies of NMDA receptor antagonists in animals and humans. Schizophr. Bull. *38*, 942–949.

Mohn, A.R., Gainetdinov, R.R., Caron, M.G., and Koller, B.H. (1999). Mice with reduced NMDA receptor expression display behaviors related to schizophrenia. Cell *98*, 427–436.

Moore, H., Geyer, M.A., Carter, C.S., and Barch, D.M. (2013). Harnessing cognitive neuroscience to develop new treatments for improving cognition in schizophrenia: CNTRICS selected cognitive paradigms for animal models. Neurosci. Biobehav. Rev. *37*, 2087–2091.

Morris, J.K., Honea, R.A., Vidoni, E.D., Swerdlow, R.H., and Burns, J.M. (2014). Is Alzheimer's disease a systemic disease? Biochim. Biophys. Acta - Mol. Basis Dis. *1842*, 1340–1349.

Muhammad, S., Barakat, W., Stoyanov, S., Murikinati, S., Yang, H., Tracey, K.J., Bendszus, M., Rossetti, G., Nawroth, P.P., Bierhaus, A., et al. (2008). The HMGB1 receptor RAGE mediates ischemic brain damage. J. Neurosci. *28*, 12023–12031.

Murugan, M., Jang, H.J., Park, M., Miller, E.M., Cox, J., Taliaferro, J.P., Parker, N.F., Bhave, V., Hur, H., Liang, Y., et al. (2017). Combined Social and Spatial Coding in a Descending Projection from the Prefrontal Cortex. Cell *171*, 1663–1677.e16.

Nagahama, Y., Okina, T., Suzuki, N., Matsuzaki, S., Yamauchi, H., Nabatame, H., and Matsuda, M. (2003). Factor structure of a modified version of the Wisconsin Card Sorting Test: An analysis of executive deficit in Alzheimer's disease and mild cognitive impairment. Dement. Geriatr. Cogn. Disord. *16*, 103–112.

Nestor, J., Arinuma, Y., Huerta, T.S., Kowal, C., Nasiri, E., Kello, N., Fujieda, Y., Bialas, A., Hammond, T., Sriram, U., et al. (2018). Lupus antibodies induce behavioral changes mediated by microglia and blocked by ACE inhibitors. J. Exp. Med. *215*.

Newton, D.F., Naiberg, M.R., Andreazza, A.C., Scola, G., Dickstein, D.P., and Goldstein, B.I. (2017). Association of Lipid Peroxidation and Brain-Derived Neurotrophic Factor with Executive Function in Adolescent Bipolar Disorder. Psychopharmacology (Berl). *234*, 647–656.

Nowak, D.E., Tian, B., and Brasier, A.R. (2005). Two-step cross-linking method for identification of NF-κB gene network by chromatin immunoprecipitation. Biotechniques *39*, 715–724.

Orlovska-Waast, S., Köhler-Forsberg, O., Brix, S.W., Nordentoft, M., Kondziella, D., Krogh, J., and Benros, M.E. (2019). Cerebrospinal fluid markers of inflammation and infections in schizophrenia and affective disorders: a systematic review and meta-analysis. Mol. Psychiatry *24*, 869–887.

Paoletti, P., Bellone, C., and Zhou, Q. (2013). NMDA receptor subunit diversity: Impact on receptor properties, synaptic plasticity and disease. Nat. Rev. Neurosci. *14*, 383–400.

Pedrazzi, M., Averna, M., Sparatore, B., Patrone, M., Salamino, F., Marcoli, M., Maura, G., Cervetto, C., Frattaroli, D., Pontremoli, S., et al. (2012). Potentiation of NMDA Receptor-

Dependent Cell Responses by Extracellular High Mobility Group Box 1 Protein. PLoS One *7*.

Plessow, F., Fischer, R., Kirschbaum, C., and Goschke, T. (2011). Inflexibly focused under stress: Acute psychosocial stress increases shielding of action goals at the expense of reduced cognitive flexibility with increasing time lag to the stressor. J. Cogn. Neurosci. *23*, 3218–3227.

Pnevmatikakis, E.A., Soudry, D., Gao, Y., Machado, T.A., Merel, J., Pfau, D., Reardon, T., Mu, Y., Lacefield, C., Yang, W., et al. (2016). Simultaneous Denoising, Deconvolution, and Demixing of Calcium Imaging Data. Neuron *89*, 285.

Prinz, M., and Priller, J. (2014). Microglia and brain macrophages in the molecular age: From origin to neuropsychiatric disease. Nat. Rev. Neurosci. *15*, 300–312.

Ronfani, L., Ferraguti, M., Croci, L., Ovitt, C.E., Schöler, H.R., Consalez, G.G., and Bianchi, M.E. (2001). Reduced fertility and spermatogenesis defects in mice lacking chromosomal protein Hmgb2. Development *128*, 1265–1273.

Ruepp, A., Waegele, B., Lechner, M., Brauner, B., Dunger-Kaltenbach, I., Fobo, G., Frishman, G., Montrone, C., and Mewes, H.W. (2009). CORUM: The comprehensive resource of mammalian protein complexes-2009. Nucleic Acids Res. *38*.

Scheggia, D., Bebensee, A., Weinberger, D.R., and Papaleo, F. (2014). The ultimate intra-/extra-dimensional attentional set-shifting task for mice. Biol. Psychiatry *75*, 660–670.

Semenza, G.L., Roth, P.H., Fang, H.M., and Wang, G.L. (1994). Transcriptional regulation of genes encoding glycolytic enzymes by hypoxia-inducible factor 1. J. Biol. Chem. *269*, 23757–23763.

Sen, N., Hara, M.R., Kornberg, M.D., Cascio, M.B., Bae, B. Il, Shahani, N., Thomas, B., Dawson, T.M., Dawson, V.L., Snyder, S.H., et al. (2008). Nitric oxide-induced nuclear GAPDH activates p300/CBP and mediates apoptosis. Nat. Cell Biol. *10*, 866–873.

Shahani, N., and Sawa, A. (2011). Nitric oxide signaling and nitrosative stress in neurons: Role for S-nitrosylation. Antioxidants Redox Signal. *14*, 1493–1504.

Shi, Y., Guo, X., Zhang, J., Zhou, H., Sun, B., and Feng, J. (2018). DNA binding protein HMGB1 secreted by activated microglia promotes the apoptosis of hippocampal neurons in diabetes complicated with OSA. Brain. Behav. Immun. *73*, 482–492.

Sochocka, M., Diniz, B.S., and Leszek, J. (2017). Inflammatory Response in the CNS: Friend or Foe? Mol. Neurobiol. *54*, 8071–8089.

Stokes, M.G., Buschman, T.J., and Miller, E.K. (2017). Dynamic Coding for Flexible Cognitive Control. In The Wiley Handbook of Cognitive Control, pp. 221–241.

Štros, M. (2010). HMGB proteins: Interactions with DNA and chromatin. Biochim. Biophys.

Acta - Gene Regul. Mech. *1799*, 101–113.

Tamura, T., Yanai, H., Savitsky, D., and Taniguchi, T. (2008). The IRF Family Transcription Factors in Immunity and Oncogenesis. Annu. Rev. Immunol. *26*, 535–584.

Tanaka, T., Matsuda, T., Hayes, L.N., Yang, S., Rodriguez, K., Severance, E.G., Yolken, R.H., Sawa, A., and Eaton, W.W. (2017). Infection and inflammation in schizophrenia and bipolar disorder. Neurosci. Res. *115*, 59–63.

Tristan, C., Shahani, N., Sedlak, T.W., and Sawa, A. (2011). The diverse functions of GAPDH: Views from different subcellular compartments. Cell. Signal. *23*, 317–323.

Upthegrove, R., and Khandaker, G.M. (2020). Cytokines, Oxidative Stress and Cellular Markers of Inflammation in Schizophrenia. Curr. Top. Behav. Neurosci. *44*, 49–66.

Yu, X., and Li, S. (2017). Non-metabolic functions of glycolytic enzymes in tumorigenesis. Oncogene *36*, 2629–2636.

Zhang, M., Kariya, T., Genri, N., Sasaki, H., Sasaki, M., Ramos, A., Nakamura, S., Iwakiri, M., Koitabashi, N., Zhu, G., et al. (2022). Nuclear GAPDH cascade mediates pathological cardiac hypertrophy. bioRxiv doi: 10.1101/844902

Zhou, P., Resendez, S.L., Rodriguez-Romaguera, J., Jimenez, J.C., Neufeld, S.Q., Giovannucci,

A., Friedrich, J., Pnevmatikakis, E.A., Stuber, G.D., Hen, R., et al. (2018). Efficient and accurate extraction of in vivo calcium signals from microendoscopic video data. Elife *7*.

FIGURE 1

A

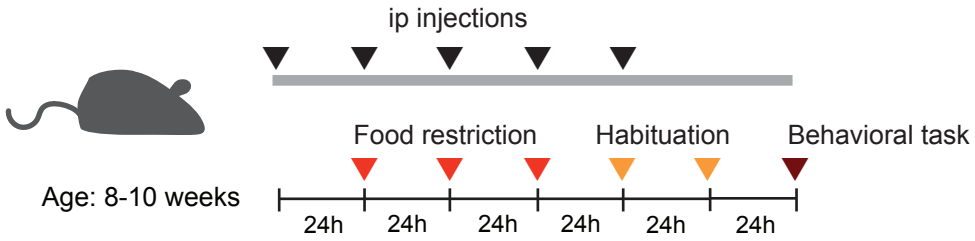

B

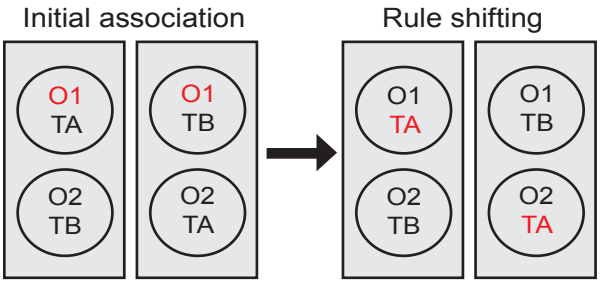

C

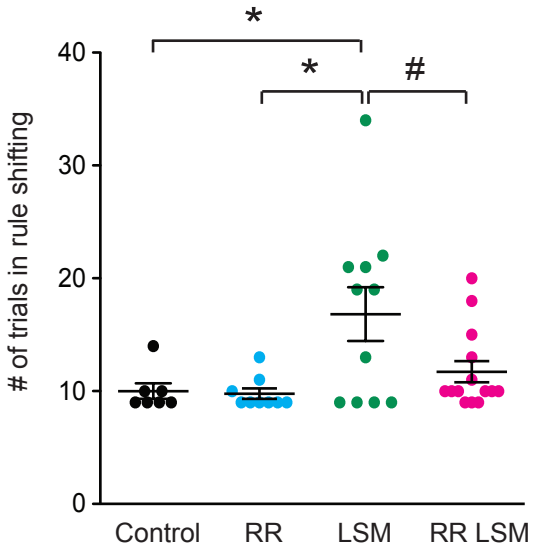

D

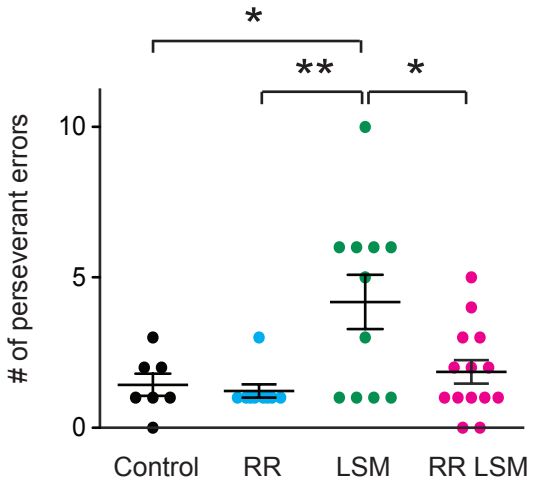

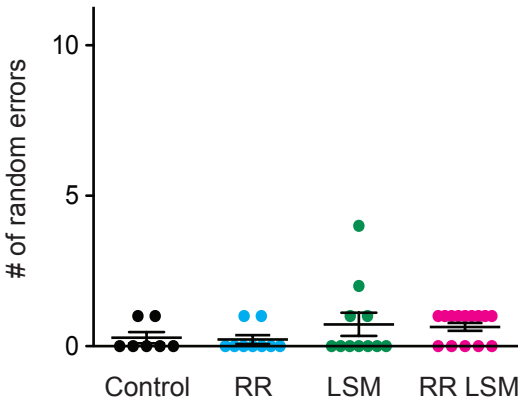

FIGURE 2

A

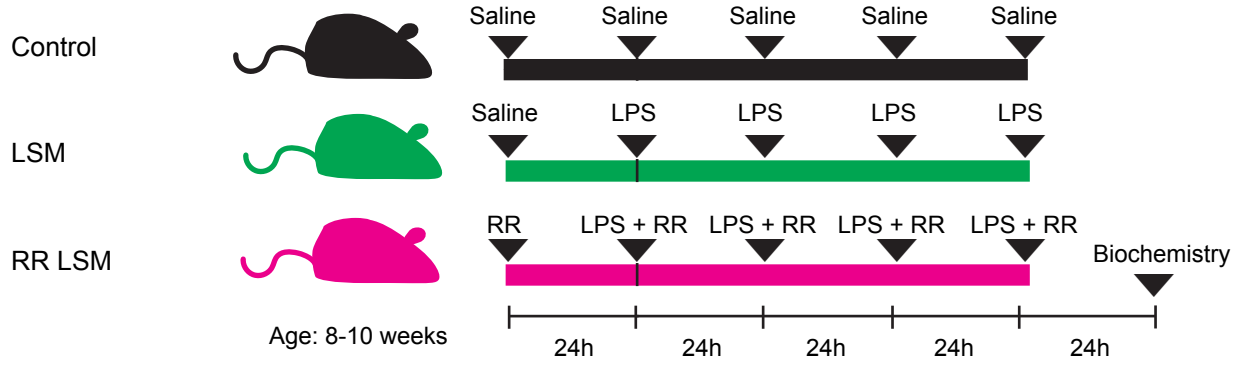
Control
LSM
RR LSM
Saline
Saline
Saline
Saline
Saline
Saline
LPS
LPS
LPS
LPS
RR
LPS + RR
LPS + RR
LPS + RR
LPS + RR
Biochemistry
Age: 8-10 weeks
24h
24h
24h
24h
24h

B

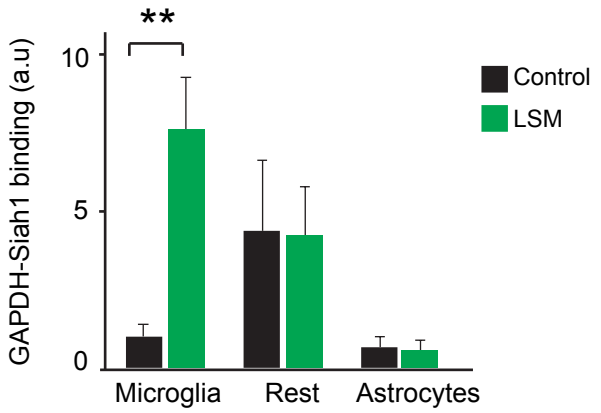
**
GAPDH-Siah1 binding (a.u)
10
5
0
Control
LSM
Microglia
Rest
Astrocytes

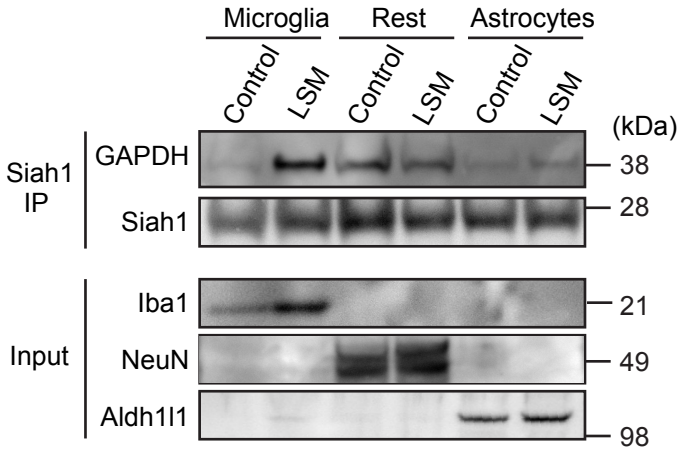
Microglia
Rest
Astrocytes
Control
LSM
Control
LSM
Control
LSM
(kDa)
Siah1 IP
GAPDH
Siah1
38
28
Input
Iba1
NeuN
Aldh1l1
21
49
98

C

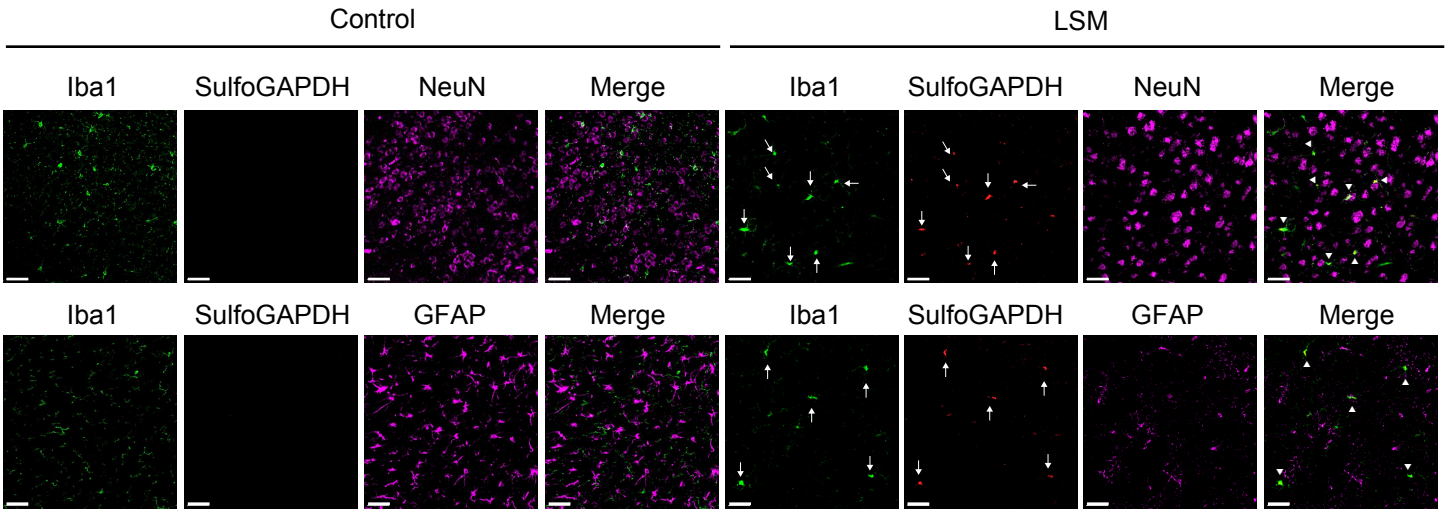
Control
LSM
Iba1
SulfoGAPDH
NeuN
Merge
Iba1
SulfoGAPDH
NeuN
Merge
Iba1
SulfoGAPDH
GFAP
Merge
Iba1
SulfoGAPDH
GFAP
Merge

FIGURE 2

D

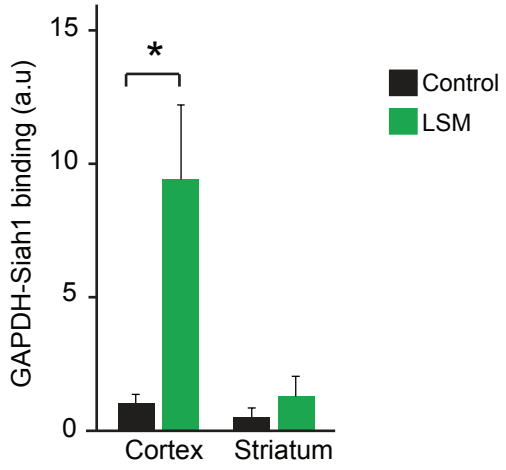

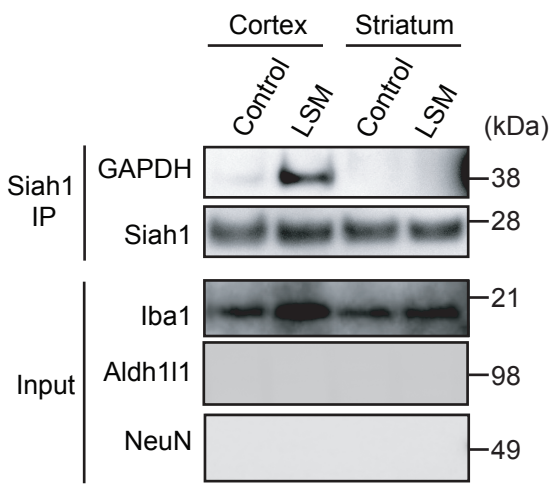

E

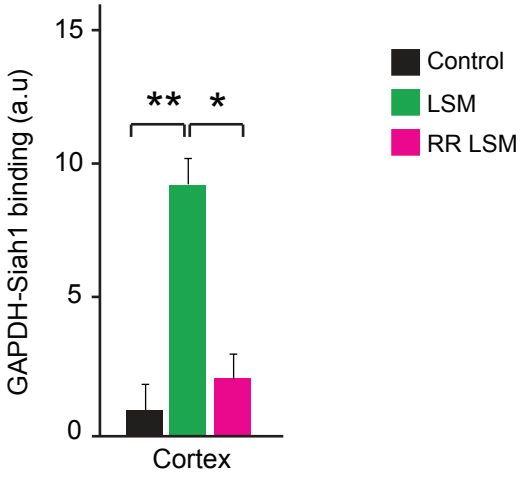

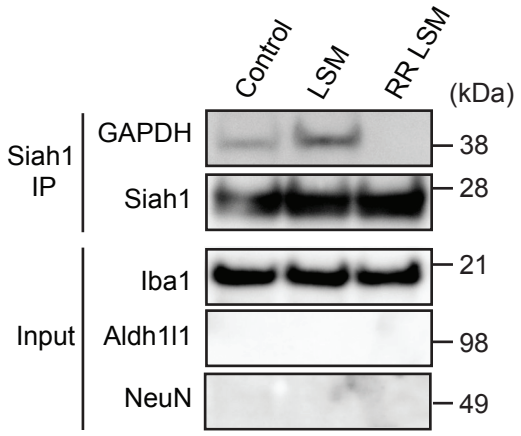

F

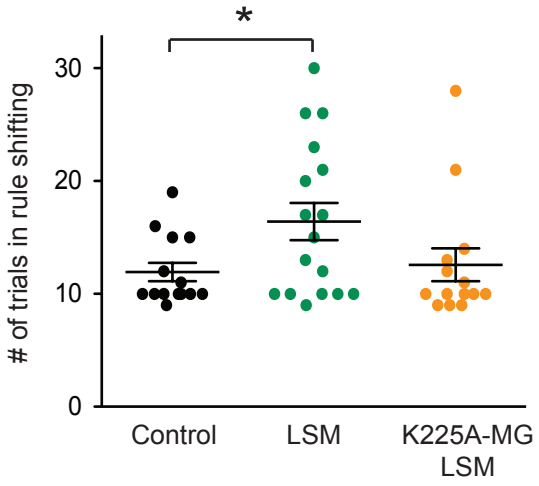

G

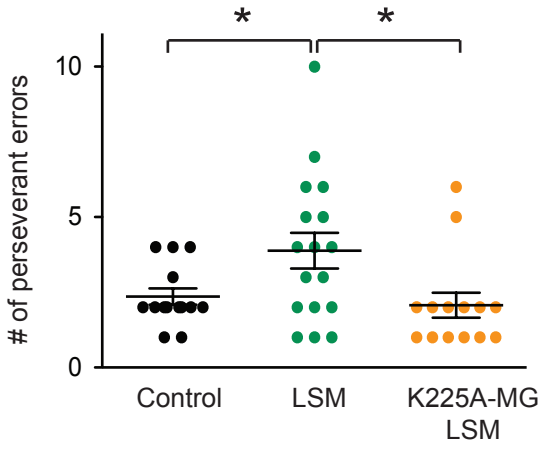

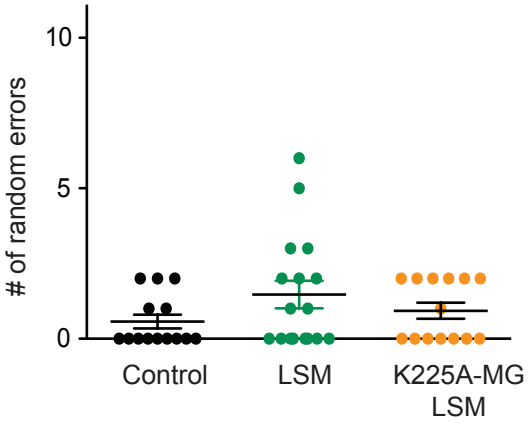

FIGURE 3

A

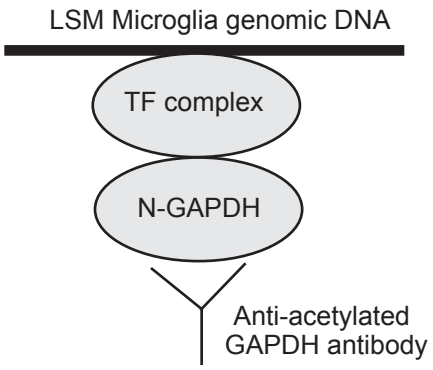

TF: Transcription factor

B

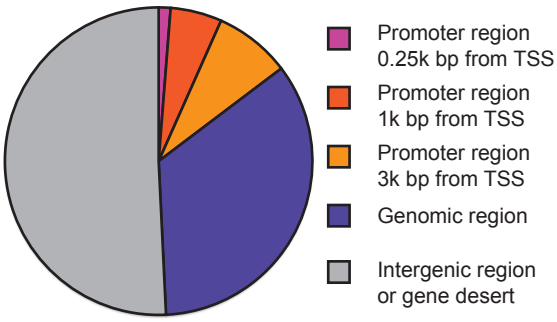

TSS: Transcription starting site
Total number of peaks identified: 721

C

Motif sequence	E value	Similar motifs	p value
	9.2×10^{-621}	STAT1	3.33×10^{-6}
	1.1×10^{-621}	FOXJ3	4.29×10^{-5}
	1.1×10^{-112}	SMCA5	8.22×10^{-10}
	1.2×10^{-116}	SALL1	1.57×10^{-5}
	1.2×10^{-116}	NR1D1	9.28×10^{-4}

D

Motif sequence	E value	Similar motifs	Region matches
	1.7×10^{-41}	STAT1	573
	9.0×10^{-35}	STAT2	486
	1.1×10^{-32}	FOXJ3	476
	3.8×10^{-32}	IRF3	508
	1.2×10^{-30}	IRF2	456

E

Ingenuity canonical pathways	- log (p value)	Molecules
Unfolded protein response	3.28	HSPA14, UBXN4, XBP1, ATF6, MAP3K5
Endoplasmic reticulum stress pathway	2.71	XBP1, ATF6, MAP3K5
Glycolysis and NADH production	2.41	GAPDH, Pgk1, Ldhc
HMGB signaling	2.25	MAP2K6, KAT2B, HAT1, IL17F, NFKB1, FNBP1, HMGB2
Sumoylation pathway	2.10	CREBBP, FNBP1, MAP3K5, NFKB1

FIGURE 4

A

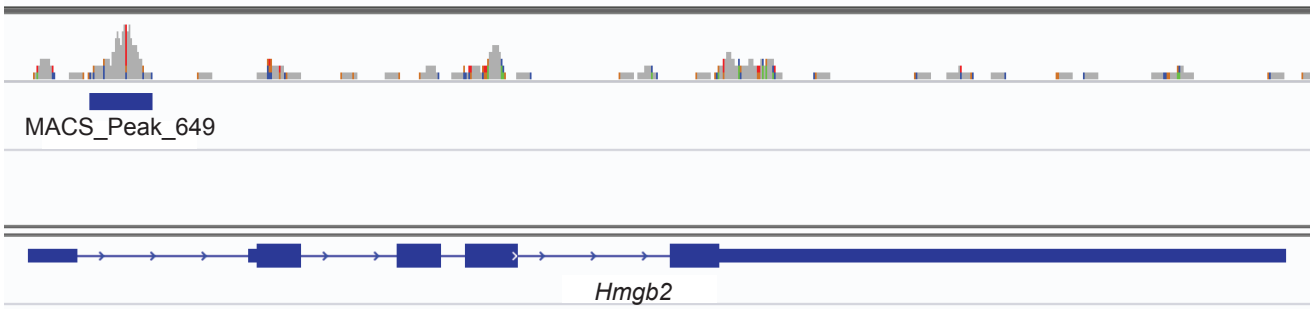

B

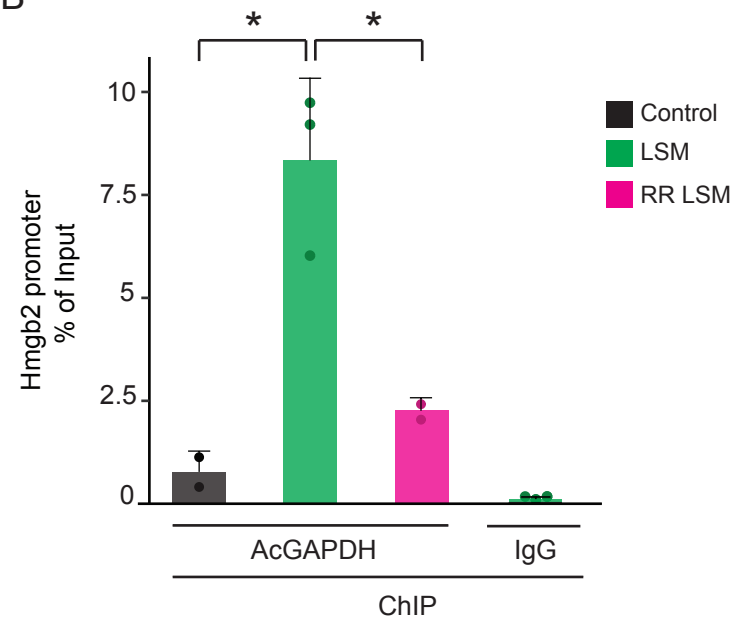

C

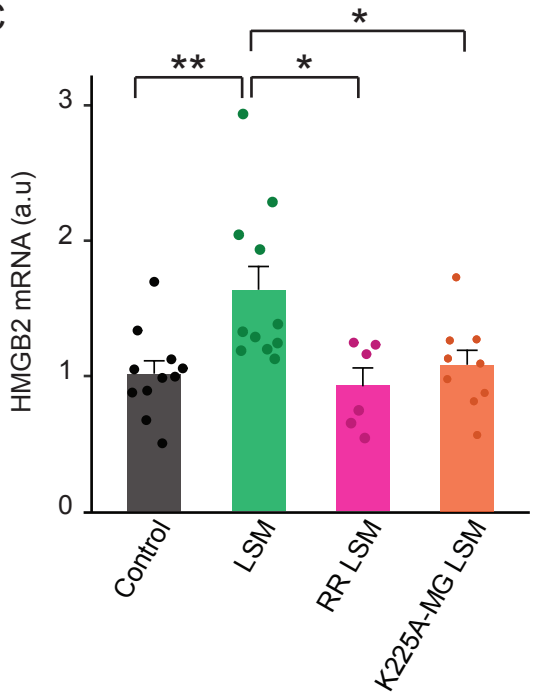

D

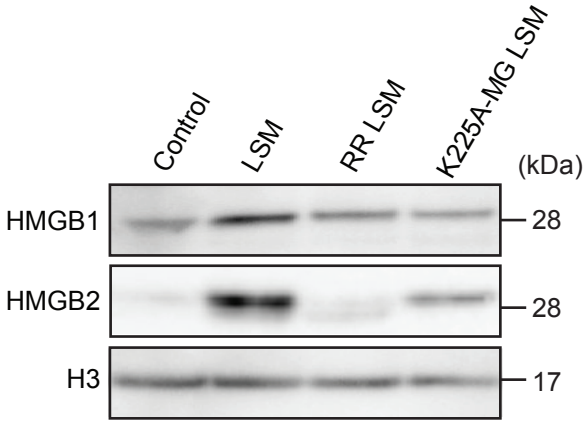

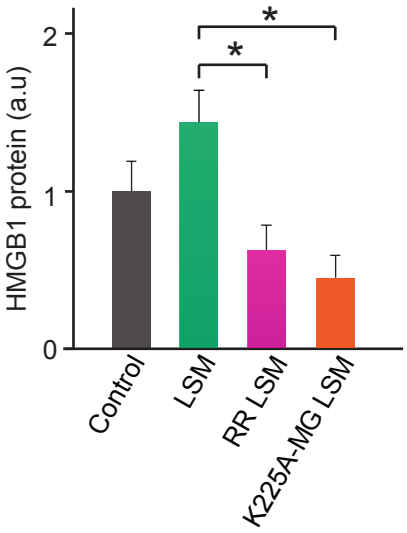

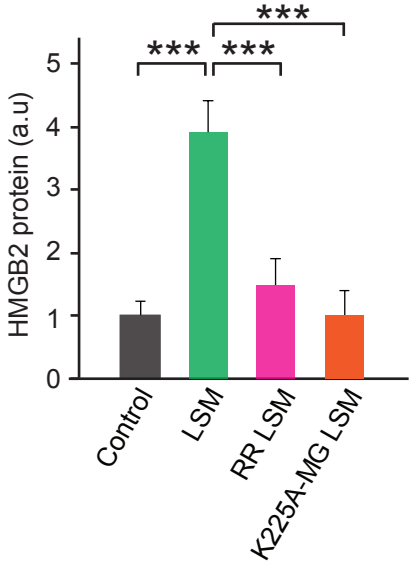

FIGURE 4

E

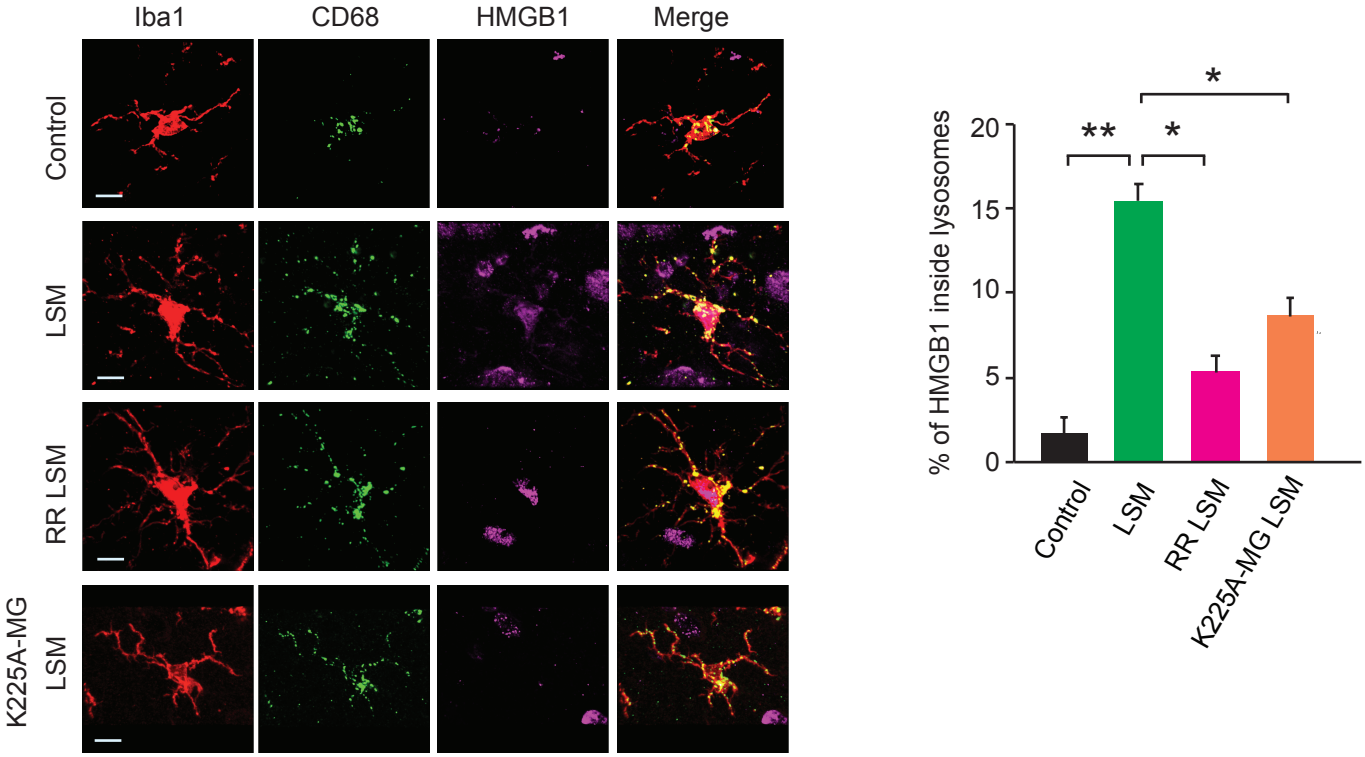
Iba1
CD68
HMGB1
Merge
Control
LSM
RR LSM
K225A-MG LSM
% of HMGB1 inside lysosomes
20
15
10
5
0
**
*
*
Control
LSM
RR LSM
K225A-MG LSM

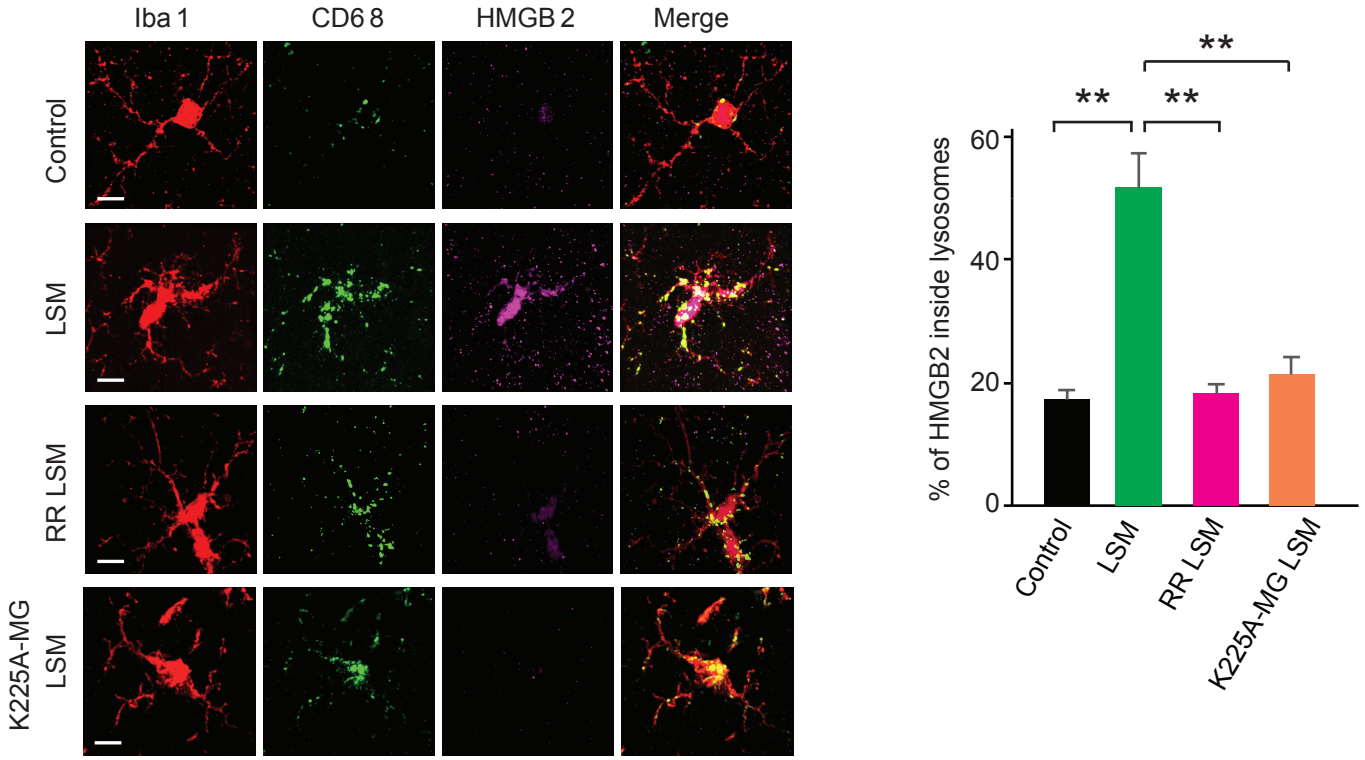
Iba 1
CD6 8
HMGB 2
Merge
Control
LSM
RR LSM
K225A-MG LSM
% of HMGB2 inside lysosomes
60
40
20
0
**
**
**
Control
LSM
RR LSM
K225A-MG LSM

FIGURE 5

A

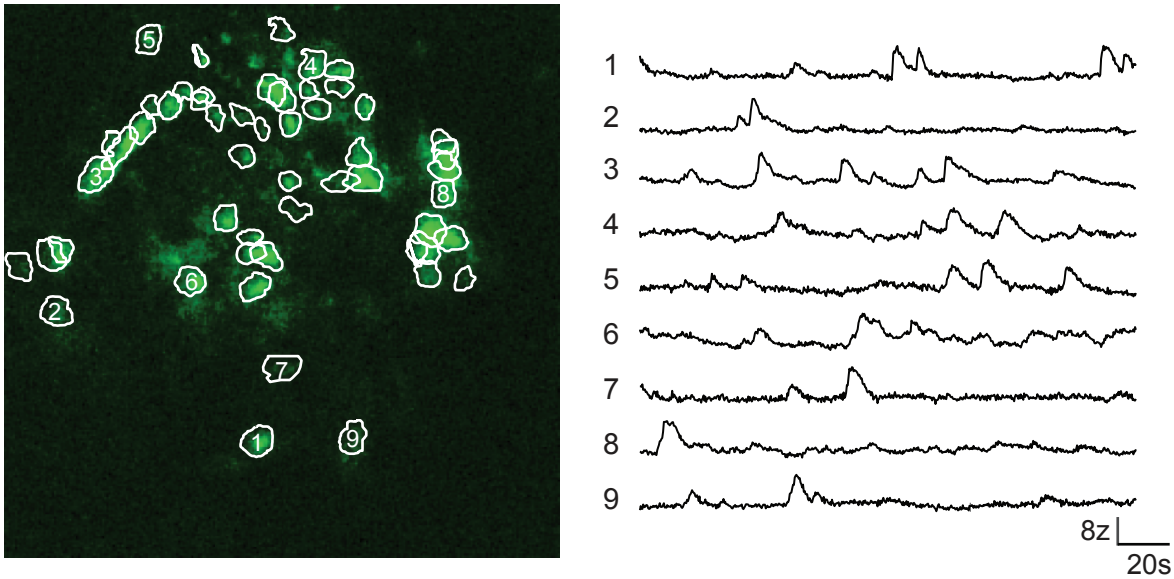

B

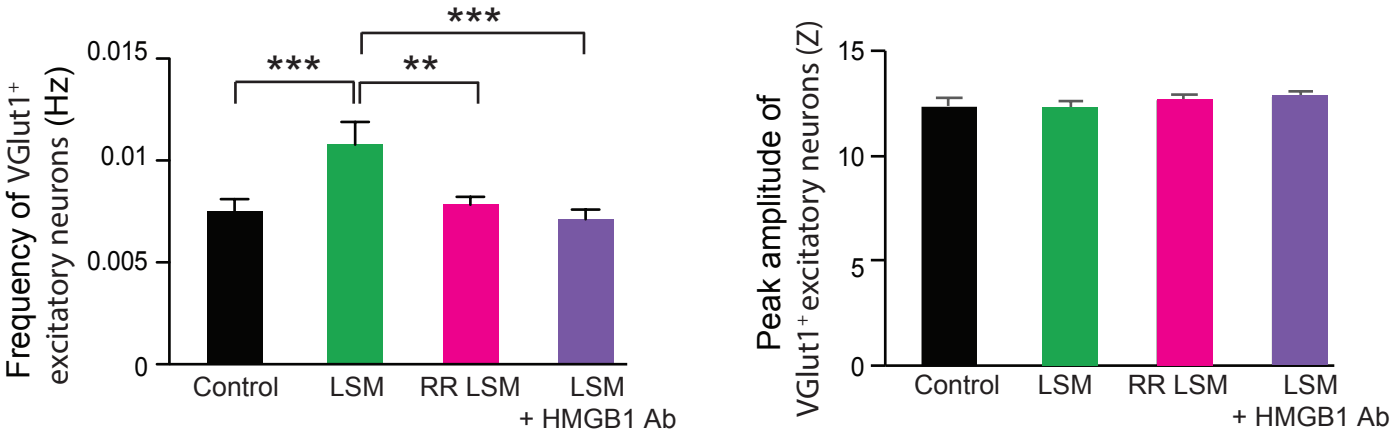

C

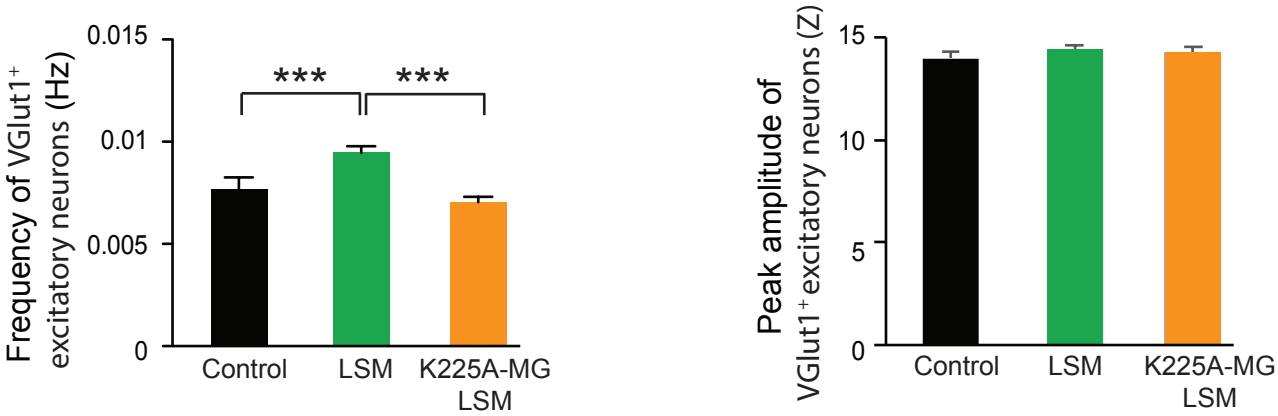

D

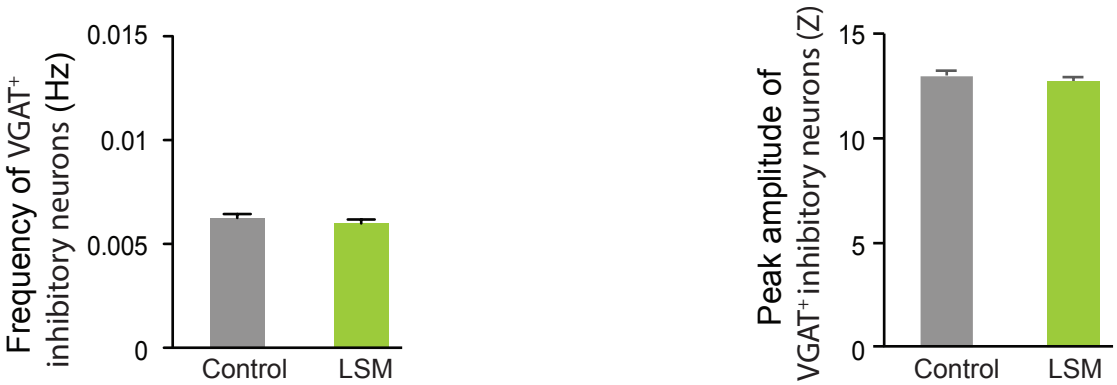

FIGURE 5

E

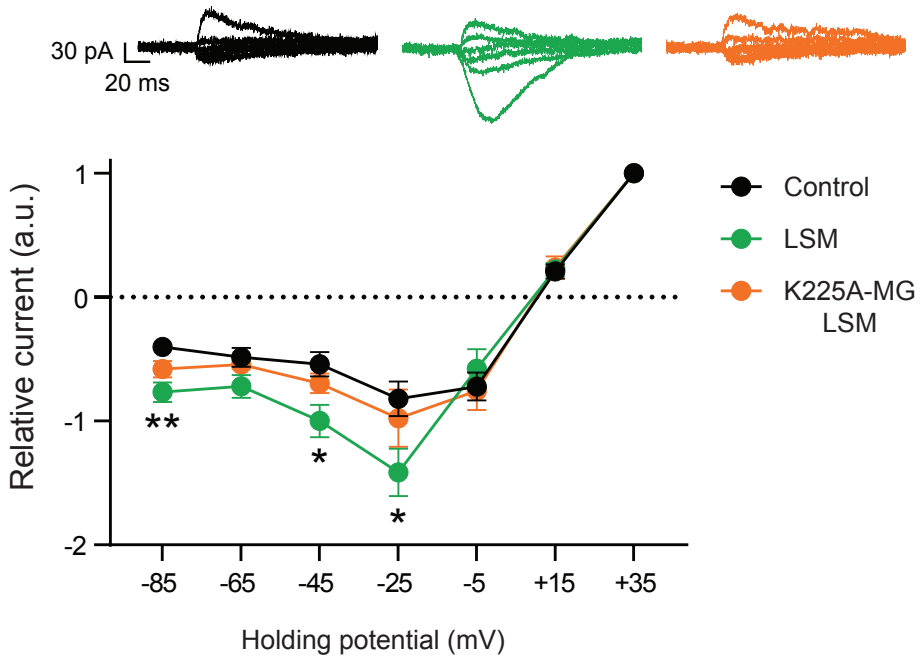
30 pA
20 ms
Relative current (a.u.)
1
0
-1
-2
**
*
*
-85
-65
-45
-25
-5
+15
+35
Holding potential (mV)
Control
LSM
K225A-MG
LSM

FIGURE 6

A

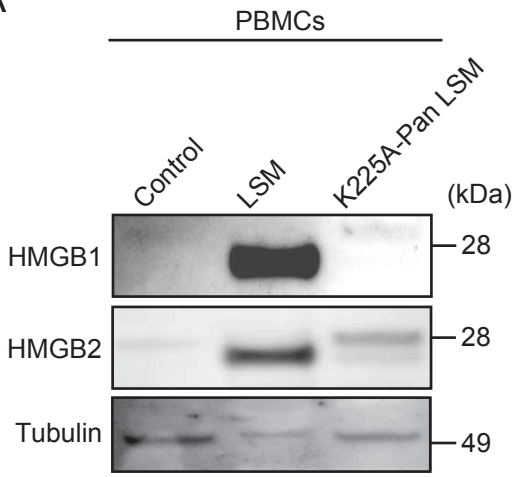
PBMCs
Control
LSM
K225A-Pan LSM
(kDa)
HMGB1
28
HMGB2
28
Tubulin
49

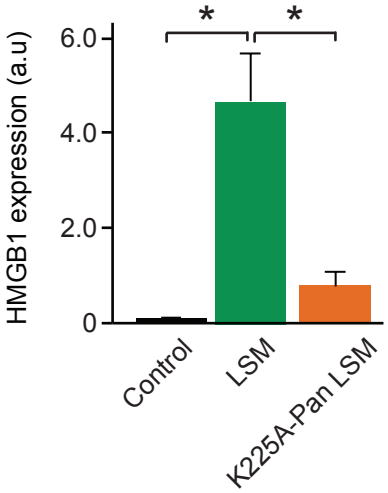
HMGB1 expression (a.u)
6.0
4.0
2.0
0
*
*
Control
LSM
K225A-Pan LSM

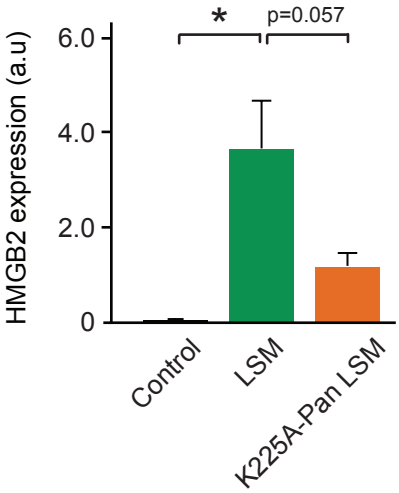
HMGB2 expression (a.u)
6.0
4.0
2.0
0
*
p=0.057
Control
LSM
K225A-Pan LSM

B

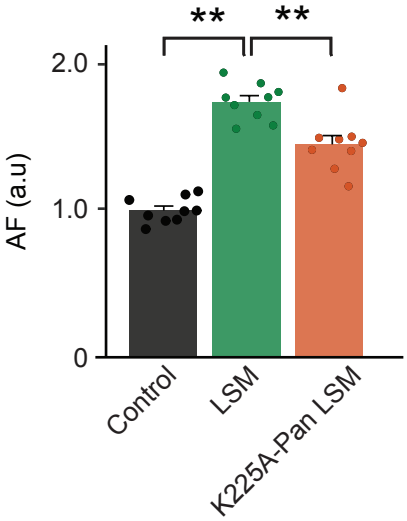
AF (a.u)
2.0
1.0
0
**
**
Control
LSM
K225A-Pan LSM

C

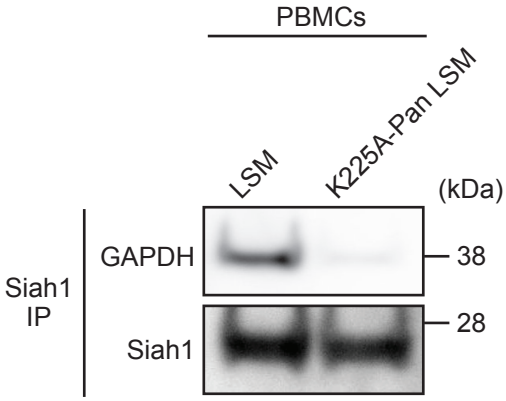
PBMCs
LSM
K225A-Pan LSM
(kDa)
Siah1
IP
GAPDH
38
Siah1
28

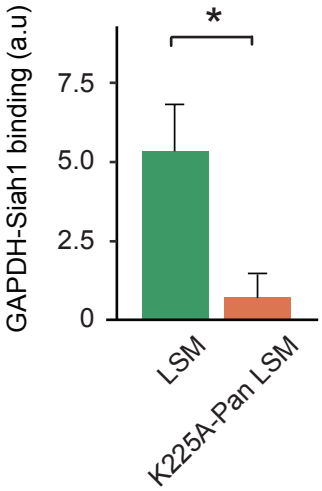
GAPDH-Siah1 binding (a.u)
7.5
5.0
2.5
0
*
LSM
K225A-Pan LSM

FIGURE 7

A

	Control	SZ	p value
Number	33	34	
Age (mean)	35.15	35.20	0.984
Gender (M/F)	25/8	25/9	0.984
Race			0.870
AA	22	21	
Cauc	9	11	
Other	2	2	
Smoker	12	18	0.263
Education (mean)	12.88	12.18	0.250
IQ (mean)	101.17	97.58	0.278

B

AF			
	β (effect size)	p value	Sample Size
Executive function			
Unadjusted	-0.08749	0.020	67
Adjusted	-0.08910	0.020	67
Attention/ working memory			
Unadjusted	0.06404	0.231	30
Adjusted	0.03811	0.452	30
Verbal memory			
Unadjusted	-0.05329	0.180	66
Adjusted	-0.01503	0.689	66
Visual memory			
Unadjusted	-0.04475	0.324	66
Adjusted	-0.03001	0.548	66
Processing speed			
Unadjusted	-0.02314	0.532	64
Adjusted	-0.00290	0.930	64
Ideational fluency			
Unadjusted	-0.04343	0.219	66
Adjusted	-0.01736	0.591	66

C

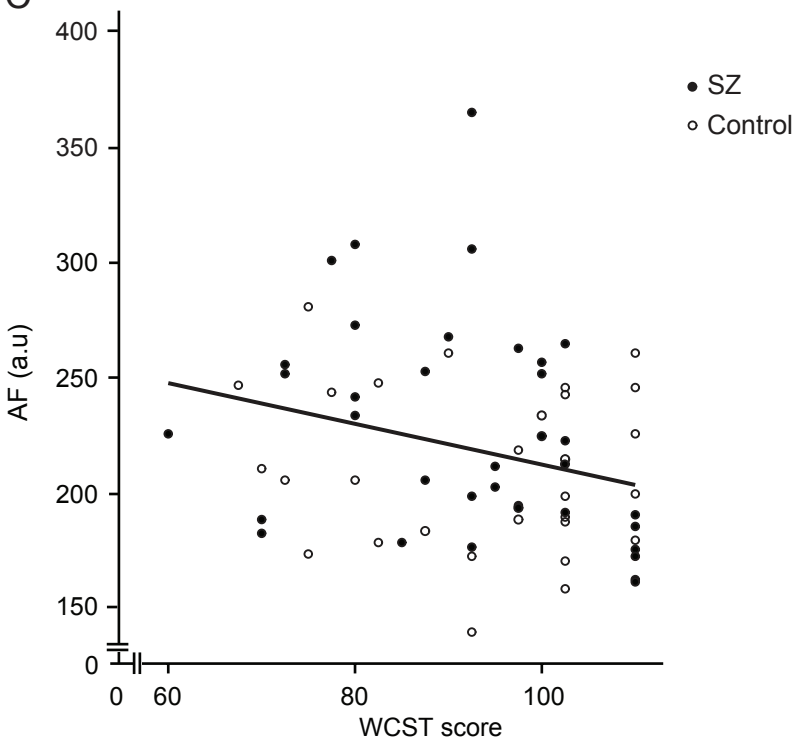

D

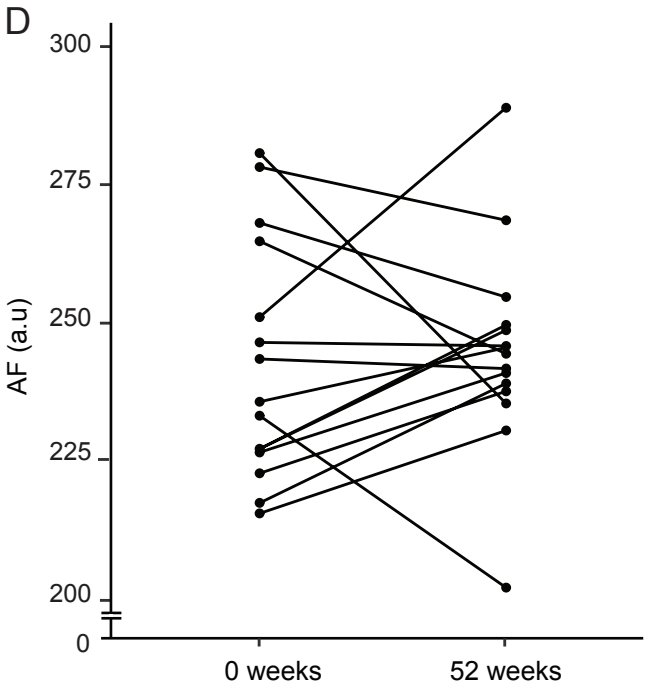
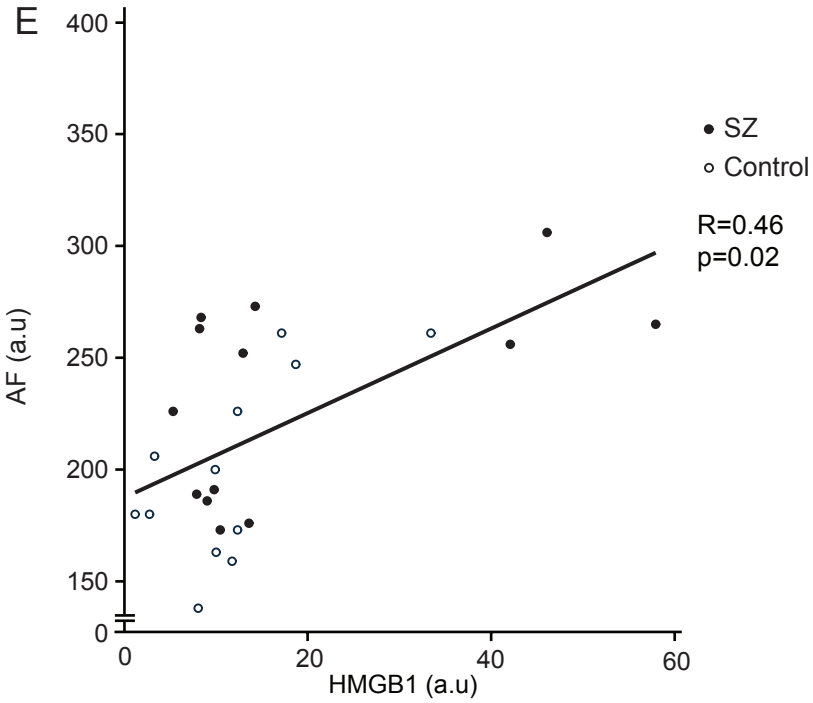
E